Studying *miR-34a* mediated gene regulation during hepatic embryogenesis

Madalena Pereira de Freitas

Thesis to obtain the Master of Science Degree in

Biotechnology

Supervisors:

Dr. Paulina Zydowicz-Machtel

Dr. Tiago Paulo Gonçalves Fernandes

Examination Committee

Chairperson: Professor Cláudia Alexandra Martins Lobato da Silva

Supervisor: Dr. Paulina Zydowicz-Machtel

Members of the Committee: Dr. Mariana da Mota Veiga de Araújo Branco

October 2022

Preface

The work presented in this thesis was performed at the Department of Cell and Molecular Biology of Karolinska Institutet (Stockholm, Sweden), during the period February-August 2022, under the supervision of Dr. Paulina Zydowicz-Machtel, and within the frame of the Erasmus programme. The thesis was co-supervised at Instituto Superior Técnico by Dr. Tiago Paulo Gonçalves Fernandes.

Declaration

Declaro que o presente documento é um trabalho original da minha autoria e que cumpre todos os requisitos do Código de Conduta e Boas Práticas da Universidade de Lisboa.

I declare that this document is an original work of my own authorship and that it fulfils all the requirements of the Code of Conduct and Good Practices of the Universidade de Lisboa.

Acknowledgements

Firstly, I want to thank all the members of the Emma R. Andersson research group at Karolinska Institutet, Sweden. Each element had a significant role during my adaptation and learning while abroad. I want to give a special thank you to Emma Andersson for teaching me how to think like a researcher and how to ask the right questions at the right time. I also want to thank Elisabeth Verboven, for supporting me, giving me advice and welcoming me as a friend. Furthermore, I want to express my sincere gratitude to Paulina Zydowicz-Machtel. Throughout my stay in Sweden, she supported me in the good and bad times. Even when things got difficult, I did not doubt my work because she was by my side. She helped me grow as a professional and as a person. It is my pleasure to have worked with this research group, it was a unique and honourable experience. I also want to thank Professor Tiago Fernandes from Instituto Superior Técnico for his availability and support.

Secondly, I want to thank my family for all the support and guidance throughout this process. Especially my father for all the advice and strength he has given me. My brother and sister for all the long conversations that made me feel closer to home. A special thank you to my grandmother for having the patience to listen to me every day. Lastly, I want to thank my boyfriend, that made sure I never felt alone during this journey.

Abstract

Millions of cells emerge, differentiate, and die from embryonic development to adulthood. This is controlled by regulatory mechanisms, such as miRs (microRNAs), that ensure accurate gene expression. Their failure leads to developmental and post-natal disorders such as liver diseases. Globally, around 2 million deaths result from liver pathogenesis each year. Additionally, several liver developmental illnesses are, to this date, untreated, but efforts are being made to develop efficient therapeutics to cure them. Subsequently, this study uses miRs, regulators of gene expression, to target *Notch2* and *Hnf4α*, genes essential during liver development and pathogenesis. The analysis was performed in the mouse E13.5 (embryonic day 13.5) hepatoblasts to mimic hepatic development. These cells were transfected with *miR-34a*, a regulator of these two genes. Seven chemically modified *miR-34a* variants were tested to surpass transfection limitations and determine which modifications lead to more effective downregulation of the target genes. In this study, the *miR-34a* variants were encapsulated with lipid nanoparticles (LNPs) as a transfection agent. The RT-qPCR method (reverse transcription quantitative PCR) was used to measure the downregulation efficiency. With the attained results, 48h was established as the best transfection and downregulation time for the tested *miR-34a* variants transfected with LNPs (*miR-34a*-LNP). It was also possible to observe that among all the tested modifications of *miR-34a*-LNP, phosphorylation at the 5'-end with one phosphorothioate bond at each molecule's end leads to higher transfection and downregulation efficiencies. Together these results take nucleic acid therapeutics one step further, primarily in battling hepatic developmental and perinatal disorders.

Keywords: liver development, *miR-34a*, LNPs, *Hnf4α*, *Notch2*.

Resumo

Desde a embriogénese até a vida adulta, milhões de células emergem, diferenciam-se e morrem. Este fenómeno é controlado por mecanismos regulatórios, como microRNAs, que garantem uma correta expressão genética. A falhas destes, leva ao desenvolvimento de patologias embrionárias e pós-natais como doenças hepáticas. Anualmente, 2 milhões de mortes resultam de distúrbios hepáticos. Adicionalmente, várias doenças hepáticas estão, até hoje, sem cura. Contudo, muitos esforços estão a ser feitos para desenvolver tratamentos para ditas doenças. Este estudo usa microRNAs para regular a expressão de *Notch2* e *Hnf4α*, genes essenciais durante a embriogénese hepática. A análise foi realizada em hepatoblastos de rato no dia embrionário 13.5, de forma a mimetizar o desenvolvimento hepático. Estas células foram transfectadas com *miR-34a,* um regulador de *Notch2* e *Hnf4α*. Sete variantes de *miR-34a*, que diferem entre si por modificações químicas, foram testadas para ultrapassar limitações na transfecção e determinar que modificações levam a uma regulação mais eficiente. As variantes foram encapsuladas em nanopartículas lipídicas. A técnica RT-PCR foi usada para avaliar a eficiência desta regulação. Com base nos resultados obtidos, 48h foi estabelecido como sendo o melhor tempo de transfecção e regulação para as variantes de *miR-34a*. Foi ainda possível observar que entre as modificações testadas, uma fosforilação na extremidade 5' e uma ligação fosforotioato em cada extremo da molécula levam a uma melhor eficiência quer de transfecção quer de regulação. Deste modo, estes resultados permitem dar um passo em frente nos tratamentos com ácidos nucleicos, principalmente no combate a doenças hepáticas.

Palavras-chave: desenvolvimento embrionário do fígado, *miR-34a*, nanopartículas lipídicas, *Hnf4α*, *Notch2*.

List of Contents

List of Figures

List of Tables

List of Abbreviations

VMEL	Ventral midline of the endoderm lip
MMPs	Metalloproteinases
STM	Septum transversum mesenchyme
FGF	Fibroblast growth factor
BMP	Bone morphogenic protein-ligand
ECM	Extracellular matrix
PDS	Primitive ductal structures
miRNA	MicroRNA
XPO5	Exportin 5
DGCR8	DiGeorge Syndrome Critical Region 8
RAN	Ras-related nuclear protein
TRBP	TAR RNA binding protein
RISC	RNA-induced silencing complex
HCC	Hepatocellular carcinoma
NAFLD	Non-alcoholic fatty liver disease
NASH	Non-alcoholic steatohepatitis
ALGS	Alagille syndrome
Hnf4α	Hepatocyte nuclear factor 4α
Notch2	Notch receptor 2
Sox9	SRY-Box Transcription Factor 9
MACS	Magnetic-activated cell sorting
FBS	Fetal Bovine Serum
DMEM	Dulbecco's Modified Eagle Medium
LNP	Lipid nanoparticle
FDA	Food and Drug Administration
UTR	Untranslated region
DSPC	1,2-distearoyl-sn-glycero-3-phosphocholine
PEG	Polyethylene glycol
PO	Phosphodiester
PS	Phosphorothioate
5'-PHOS	Phosphate group at the 5' end
C_T	Cycle threshold
NTC	Non-template control

GOI	Gene of interest
RG	Reference genes
RQ	Relative gene expression
Tm	Melting temperature
SDS-PAGE	Sodium dodecyl sulfate-polyacrylamide gel electrophoresis
RT-qPCR	Reverse transcription quantitative polymerase chain reaction
TBST	Tris-buffered saline solution 0.1% Tween® 20 Detergent
H_0	Null hypothesis
H_1	Alternative hypothesis
p-value	Probability value
DLK1	Delta, like non-canonical Notch ligand 1
HGF	Hepatocyte growth factor
EGF	Epidermal growth factor
NT	Non-transfected cells
***miR-34a*-LNP**	*miR-34a* transfected with lipid nanoparticles
siRNA-*Hnf4α*-lipo	Small interfering RNA specific for *Hnf4α* transfected with lipofectamine (RNAiMAX)
scr-lipo	Scrambled *miR-34a* transfected with lipofectamine
***miR-34a*-lipo**	*miR-34a* transfected with lipofectamine
miRs-lipo	Srambled *miR-34a*, *miR-34a* and siRNA specific for *Hnf4α* transfected with lipofectamine (RNAiMAX)
scr-LNP	Scrambled *miR-34a* transfected with lipid nanoparticles
NEPTUNE	Neural plate targeting by in-utero nano injection

Introduction

1. Liver morphogenesis

1.1. Liver progenitor cells

Embryo development begins with a multistep process known as gastrulation. It entails a set of coordinated cell movements, differentiation, and proliferation that build up the three germ layers. Ectoderm lies at the periphery of the embryo, endoderm at its core and mesoderm in between [1]. As the endoderm matures, various signalling pathways and cell interactions will promote the development of distinct internal organs, such as the liver.

The liver is a pivotal organ capable of performing distinct vital biological functions from macromolecule metabolism to blood supply [2]. Thus, it is composed of multiple cell types. The two primary hepatic cell types are hepatocytes and cholangiocytes. Both originated from the liver progenitor cells known as hepatoblasts [3].

Hepatoblasts arise from two cell populations in the endoderm's ventral foregut (Fig.1) [4]. These are the ventral midline of the endoderm lip (VMEL) and the lateral endoderm cells [4]. A continuous set of hepatoblasts prevenient from the VMEL form the posterior area of the ventral gut midline and the anterior portion of the liver bud, an extension from the foregut tube. Therefore, this cell population forms a large fraction of the liver. In contrast, the lateral progenitor cells are divided into two regions, giving rise to more rostral ventral gut tissues [4,5]. At E8.5, hepatoblasts are differentiated at the ventral foregut, establishing the beginning of hepatic specification [6]. These cells will migrate and later differentiate into hepatocytes and cholangiocytes [3].

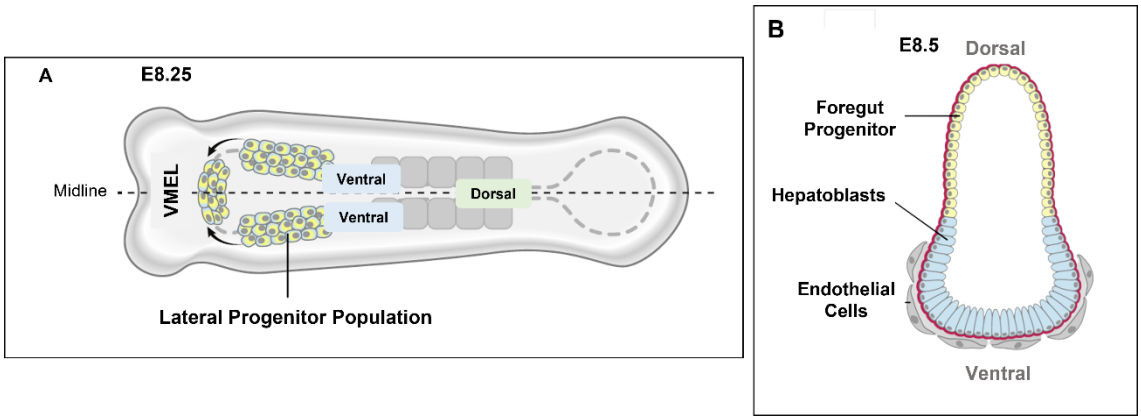

Figure 1 - Origin of hepatoblasts from progenitor cell populations in mice. A) Longitudinal view of the ventral gut with progenitor lateral and VMEL cell population at E8.25 B) Transverse view of the ventral gut with the different cell types at E8.5. Adapted from: Ober, E. A. & Lemaigre, F. P. Development of the liver: Insights into organ and tissue morphogenesis. Journal of Hepatology 68, 1049–1062 (2018).

1.2. Formation of the liver bud

After hepatic specification on the ventral foregut, the hepatoblasts proliferate and migrate to develop the liver bud [7]. There are three stages in the growth of the liver bud from the endodermal

epithelium (Fig. 2). Stage I, in mice, occurs at E8.5 and is characterised by the thickening of the epithelium at the gut lumen and the closing of the ventral gut. The intensified cell proliferation leads to hepatic endoderm elongation. This process originates a layer of cuboidal cells that comprises the apical region of the liver diverticulum from which the liver bud begins to emerge [7].

Stage II in mice arises between E9.0 and E9.5, in which the monolayer of cuboidal cells transitions into a multilayer of pseudostratified hepatoblasts [7]. The laminin surrounding the epithelium remains intact, and the nuclei of the hepatoblasts in the gut lumen begin to migrate from the apical to the basal region of the cell. This internuclear migration leads to the transition from multiple-layered stratified hepatoblasts into a single-layer pseudostratified hepatoblast [7].

Stage III, in mice, starts at E9.5 and lasts until the rest of gestation [7]. In this phase, the laminin layer disassembles, and the hepatoblasts delaminate, migrate to the septum transversum mesenchyme (STM), and start forming the liver bud [7,8]. Metalloproteinases (MMPs) are the catalytic effectors that cause laminin degradation. While the loss of contact between hepatic progenitor cells, facilitating the migration, results from the downregulation of E-cadherin [4].

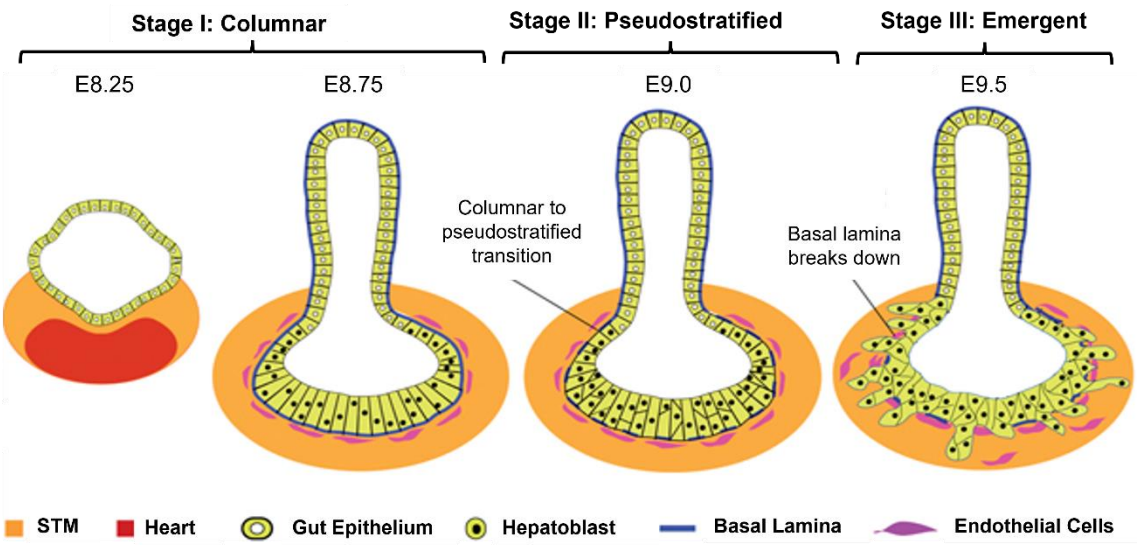

Figure 2 - Schematic representation of transverse sections of the different developmental stages during liver bud morphogenesis. At E8.5 the epithelium at the gut lumen thickens due to intense cell proliferation originating a layer of cuboidal cells. The transition from columnar to pseudostratified epithelium occurs from E8.75 to E9.0. At E9.5 the basal laminin breaks down and the hepatoblasts start to delaminate towards the STM. Adapted from: Zorn, A. M. Liver development. in (2008). doi:10.3824/stembook.1.25.1

Signalling molecules play a crucial role in hepatic specification, as they modulate hepatoblast proliferation and migration [3]. For instance, cardiac mesoderm expresses the fibroblast growth factors FGF1 and FGF2 that promote hepatic specification from the foregut in a dose-dependent manner [9]. The FGF ligands bind to the FGF1 and FGF4 receptors, expressed by ventral foregut endoderm cells. Cells' exposure to low concentrations of FGF ligands leads to albumin

upregulation, promoting liver differentiation. In contrast, when FGF ligands are highly expressed, liver-specific genes are downregulated, and lung differentiation is promoted instead [9].

Likewise, the Bone morphogenic protein-ligand (BMP) expression in the septum transversum mesenchyme leads to the activation of hepatic genes in the endoderm [10]. Mutant embryos with deletion of Bmp4 fail to thicken the foregut endoderm. This compromises liver bud morphogenesis. Moreover, the BMP signalling is essential for maintaining the expression of the transcription factor Gata4, which causes albumin upregulation, playing a vital role in the hepatic specification. [10].

Additionally, transcription factors, such as FoxA1-3, GATA4/6, Hnf6, Hex, and Prox1, play essential roles in activating hepatic genes. As such, FoxA and Prox1 are crucial gene regulators during liver development. Similarly, the GATA transcription factors play a role in embryogenesis and hepatic specification. The Hnf6 family has been correlated with hepatoblast differentiation and hepatocyte maturation. Furthermore, the Hex transcription factor is critical for liver bud development [11].

1.3. Liver lobes development

Once the liver bud has reached the septum transversum mesenchyme, it divides into four distinct lobes that vary in shape and size [4]. These variations are caused by differential cell proliferation and migration into separate sections of the liver bud [4]. The liver lobes are composed of multiple lobules, which outline the basic structural unit of the liver. The lobules have a hexagonal shape and contain a portal triad consisting of a vein, a bile duct, and a hepatic artery. The hepatocytes on the lobule are oriented according to the sinusoidal capillaries that protrude from the central vein (Fig. 3) [12]. Hence, morphogenesis must be neatly structured to ensure the correct liver architecture and generate a fully functional organ.

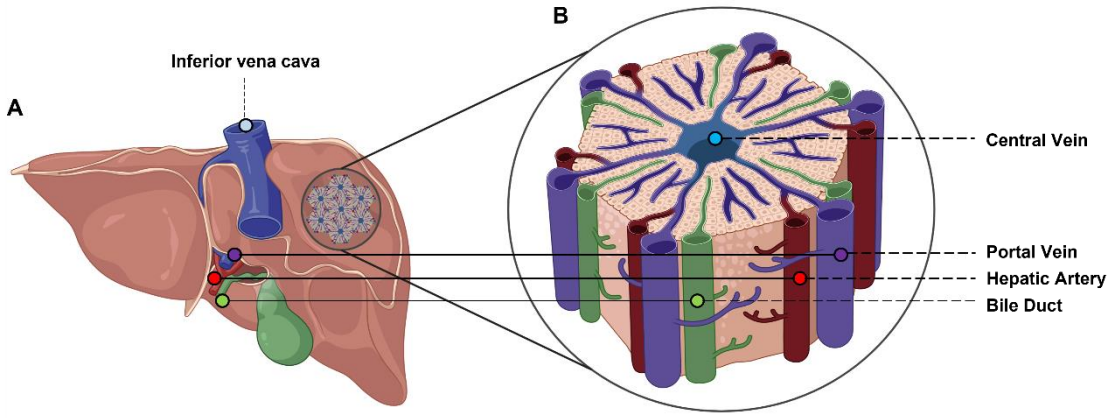

Figure 3 – Representation of the matured liver with amplification on one of its hexagonal-shaped lobules, mainly composed of hepatocytes that extend from the central vein. Each lobule also comprises a portal vein, a bile duct, and a hepatic artery, which are connected to the inferior vena cava [12].

Hepatocytes are the primary hepatic cell type taking up around 70% of the liver cell population. These cells operate in concert with cholangiocytes which cover approximately 3% of the liver cell population [12]. Hepatocytes arise from hepatoblasts in a series of complex differentiation events between E13.5 and E15.5. The process begins with a progressive silencing of cell-cycle and hepatoblast-specific genes and an increased expression of genes involved in hepatocyte functions, including metabolism, transport, and detoxification [13].

Hepatoblast differentiation into cholangiocytes represents a divergence from the default differentiation into hepatocytes [13]. Cholangiocyte specification takes place between E11.5 and E14.5. During this time, cells mainly express genes involved in standard hepatocyte functions [13]. However, from E13.5 to E17.5, cell adhesion, migration, and tube morphogenesis genes become upregulated, suggesting cholangiocyte differentiation [13]. Thus, embryonic cholangiocytes are quite heterogenous at the transcriptomic level and can perform distinct functions in different parts of the liver [3]. Furthermore, cell proliferation during hepatoblast-hepatocyte differentiation is low, whereas the percentage of proliferating cells increases during differentiation into the cholangiocyte lineage. Subsequently, hepatoblast-cholangiocyte differentiation represents an alternative branch from hepatocyte differentiation that involves distinctive regulatory mechanisms and cell proliferation rate [13].

1.4. Formation of the hepatic parenchyma

The liver is a complex organ that participates both in macromolecule metabolism and blood detoxification while also supporting the digestive and hematopoietic systems [3]. Thus, it is formed by endoderm and mesoderm-derived cells [6]. These cells communicate through signalling molecules and physical interaction, shaping the mature liver, which is sectioned into the parenchymal and non-parenchymal units [3].

The non-parenchymal cells mainly support and complement the parenchymal tissue to form a functional unit [14]. These include mesoderm-derived cells such as mesothelial cells, hepatic stellate cells, liver sinusoidal endothelial cells, and hematopoietic cells. Each cell type is responsible for an essential function that collectively ensures healthy liver activity [3].

In contrast, the liver parenchymal is the functional section of the organ composed mostly of polarised hepatocytes and, in lower amounts, cholangiocytes. The maintenance of polarised tissue requires a specific orientation throughout cell division [15]. During mitosis, hepatocytes asymmetrically orient their apical plasma membrane to the daughter cells. This asymmetric division is introduced by Par1b and Leu-Gly-Asn repeat-enriched protein that guides the mitotic spindle away from the apical membrane domain. Abnormal mitotic spindle orientation may hinder normal liver development [15].

Parenchymal liver morphology is well-structured, with hepatocytes forming a cell layer that separates endothelial sinusoids from canalicular bile. Hepatocytes are polarised cells with a basal membrane facing endothelial sinusoids and apical poles fronting one or more bile canaliculi [16]. Hepatocyte polarisation and canicular network development rely on various elements, such as

the ECM (extracellular matrix) and intracellular protein trafficking. ECM enables hepatocyte adherence and signal transduction contributing to hepatocyte differentiation. Regulation through intracellular protein trafficking, membrane sorting and endosomal recycling is needed to support hepatocyte polarity and liver functionality. Additionally, cell junctions are vital in preserving hepatocyte polarisation, as their deregulation can lead to depolarisation [16].

Liver parenchyma morphogenesis depends on several signalling pathways and transcription factors, such as Hnf4α. The hepatocyte nuclear factor (Hnf4α) is a nuclear receptor that participates in various biological functions such as metabolism, cell junctions, differentiation, and proliferation in liver cells [17]. Its capability to modulate the expression of multiple genes during liver development is crucial for normal hepatocyte differentiation [18].

As such, abnormal *Hnf4α* expression can lead to pathogenesis [17] and affect normal liver development [19]. Mice deficient in *Hnf4α* present abnormal-sized and shaped livers with irregular architecture and severe lesions [19]. These embryonic livers are structurally discontinuous and packed with large gaps filled with hematopoietic cells. The hepatocytes become small, oddly shaped, loosely linked, poor in glycogen and with a smaller cytoplasm-to-nuclei ratio. As such, the hepatic parenchyma becomes disrupted with a lack of cell proliferation [19].

1.5. Bile duct morphogenesis

The bile duct is a complex structure formed by a network of ducts responsible for the bile's transport from the liver to the duodenum. Bile is a critical component of healthy digestion comprised of bile acids, bile salts, and amino acids [20]. When bile duct morphogenesis is impaired, the embryo suffers from cholestasis, commonly followed by inflammation, fibrosis, and liver malfunction [21]. Thus, correct morphogenesis of this complex structure is mandatory.

Bile duct formation is initiated at around E15.5, marked by the lining up of cholangiocytes around the mesenchyme, forming the ductal plate (Fig. 4) [22]. This structure comprises two asymmetric lumens in a primitive ductal structures (PDS) configuration. Hepatoblasts are located on the parenchymal side, whereas cholangiocytes face the portal side. PDS represents the leading front of biliary development which occurs from the hilum to the periphery, from which hepatoblast specification into biliary cells is promoted. Once all cells in the PDS have acquired biliary characteristics, the mature ducts become symmetric. Thus, at the end of gestation, asymmetrical ducts will be gradually less predominantly from the periphery towards the hilum succumbing in a full symmetrical biliary system [22].

Signalling pathways such as *Sox9* and *Notch2* have been found to play essential roles during bile duct morphogenesis [23,24]. Sox9 is a transcription factor that regulates the expression of various genes and plays a vital role in liver development during embryogenesis [25]. At E11.5, *Sox9* starts being expressed in hepatoblasts promoting cholangiocyte differentiation and later bile duct morphogenesis. Subsequently, this gene is the first marker of cholangiocyte lineage differentiation. As such, cholangiocytes lacking *Sox9* have an impaired maturation of the ductal plate as symmetrical morphogenesis of the bile ducts is delayed [24,25].

Furthermore, the Notch pathway regulates distinct hepatic processes such as hepatocyte regeneration, biliary repair, and vascularisation maintenance [26]. Notch receptors include Notch1-4, whereas the Notch ligands are Delta-like 1, 3, 4 and Jag1-2 [27] (Jagged). These molecules are necessary for liver regeneration, repair, fibrosis, and metabolism [26]. When the Notch signalling pathway is deregulated, human disorders such as Alagille syndrome (AGLS) can be developed [26]. A study has evidence that 94.3% of the Alagille patients had mutations in the *Jagged1* gene while 2.5% had mutations in the *Notch2* gene [28]. Hence, the Notch signalling pathway is essential for maintaining a normal biliary tree density and architecture and is fundamental for normal bile duct morphogenesis, growth, and maintenance [26].

The expression of *Sox9* and the Notch receptor gene, *Notch2,* is directly co-dependent [29]. As such, Sox9 has two putative binding sites on the murine *Notch2* transcription start site. When *Sox9* is overexpressed, the levels of *Notch2* increase via direct transcription activation [29]. Thus, *Notch2* deletion in mice results in improper bile duct morphogenesis leading to structural abnormalities and compromised biliary functions. Furthermore, mutant *Notch2* mice also exhibit portal vein inflammation and fibrosis [23].

However, in postnatal model mice suffering from ALGS, the overexpression of *Sox9* results in an increase in *Notch2* expression [29]. This compensates for low levels of *Jagged1*, restoring the activity of the Notch signalling pathway, which attenuates ALGS severity. Thus, overexpression of *Sox9* promotes bile duct formation in ALGS patients by improving cholangiocyte differentiation, which may be used as therapeutics to restore bile duct paucity [29]. Hence, it is essential to understand how these signalling pathways interfere with liver development from early embryogenesis to fully mature organs.

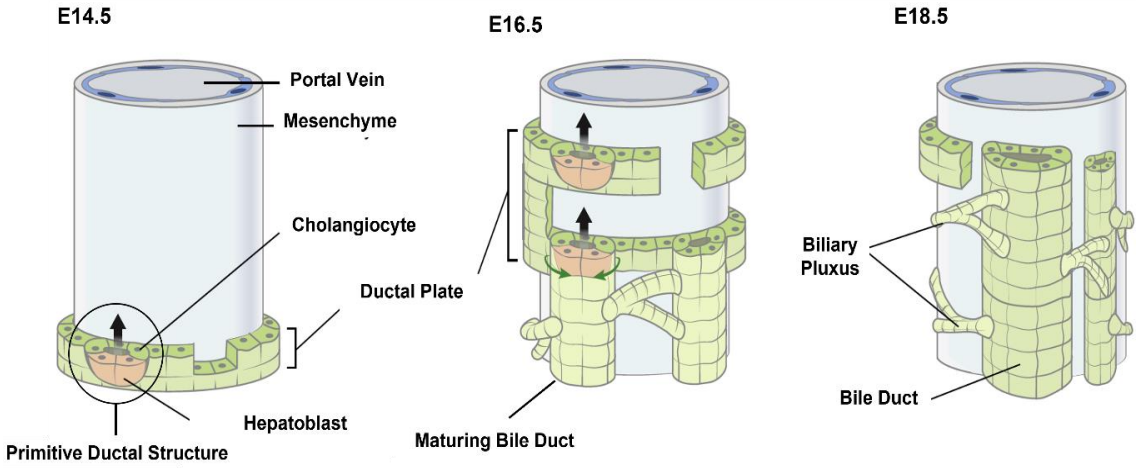

Figure 4 – Representation of bile duct morphogenesis from E14.5 to E18.5 in embryonic mouse liver. Adapted from: Ober, E. A. & Lemaigre, F. P. Development of the liver: Insights into organ and tissue morphogenesis. Journal of Hepatology 68, 1049–1062 (2018).

2. MicroRNAs

MicroRNAs (miRNAs) are small non-coding RNAs that regulate target gene expression [30]. These molecules play vital roles in cell differentiation, proliferation, and survival [30] in phylogenetically distinct organisms such as bacteria, archaea and eukarya [31]. The discovery of miRNAs dates to 1993 when in *Caenorhabditis elegans*, it was revealed that the gene *lin-4*, encoding a small non-coding RNA, could negatively regulate the expression of the protein LIN-14 affecting the developmental stages of the larvae. Currently, in *Homo sapiens,* 2654 miRNAs have been annotated in the miRNA database - miRBase (Release October 25, 2022[32]). MicroRNAs have been correlated to distinct biological functions, from cell-cell communication to human pathogenesis. Thus, it is essential to better comprehend miRNAs' regulatory effect during embryogenesis throughout liver development.

2.1. miRNAs biogenesis pathways

A functional microRNA is generated through a stepwise process that includes miRNA transcription and a set of enzymatic cleavages performed in the nucleus and in the cytoplasm [33].

In the canonical biogenesis pathway, miRNAs are firstly transcribed by RNA polymerase II as a large primary transcript named pri-miRNA [34,35] (Fig. 5). These primary molecules have at least one hairpin structure with a 5'-cap and a polyadenylation signal at the 3'-end. Afterwards, pri-miRNAs are cleaved into a 70-nucleotide pre-miRNA with a 5'-end monophosphate and a 3'-end with a two-nucleotide overhang and a stem-loop [34,35]. This processing is mediated by the microprocessor protein complex, which contains two subunits named Drosha and DiGeorge Syndrome Critical Region 8 (DGCR8) [30,36]. This cleavage's efficacy and precision determine miRNA abundance and target specificity, respectively [37–39]. After this initial maturation, the pre-miRNA is exported from the nucleus to the cytoplasm by exportin 5 (XPO5) and a Ras-related nuclear protein (RAN) [30,40].

When pre-miRNAs reach the cytoplasm, they are further processed, by Dicer and TAR RNA binding protein (TRBP), into small miRNA duplexes [30]. The miRNA duplex is loaded into the Argonaute protein, which removes the passenger strand and leaves the guide strand, the mature miRNA [30]. Subsequently, the Argonaute protein mediates the assembly of the ribonucleotide-protein complex named RNA-induced silencing complex (RISC) [35,41]. Afterwards, the Argonaute uses the miRNA sequence to identify possible mRNA targets for downregulation [42].

In the noncanonical biogenesis pathway, one or more stages of the canonical path may be bypassed [30]. These variations can be, for instance, biogenesis without the enzymatic cleavage of Drosha or Dicer. An example of a noncanonical pathway is the mirtron processing in which the Drosha and DGCR8 complex is not required [30].

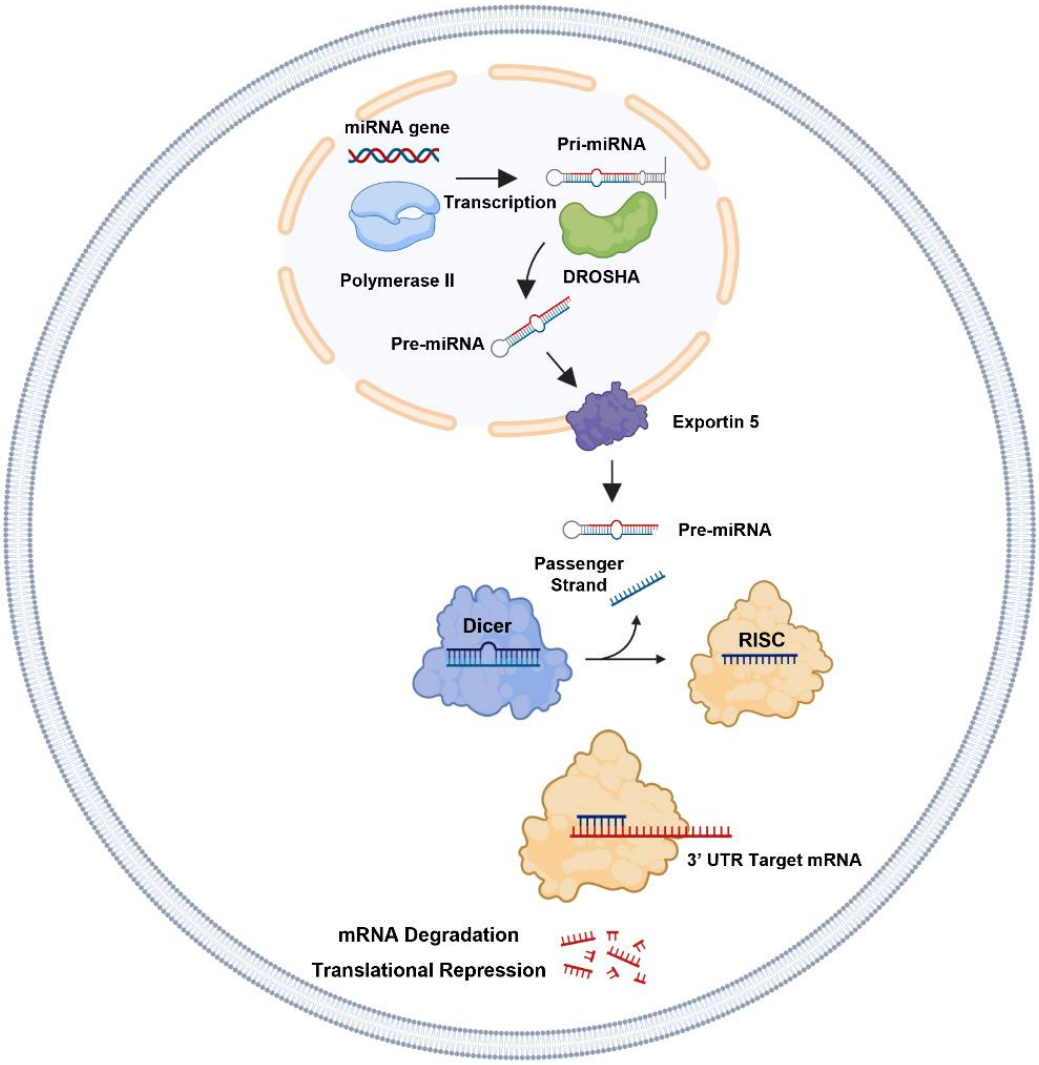

Figure 5 – Representation of the canonical biogenesis pathway of miRNA. Briefly, miRNAs are transcribed by RNA polymerase II as pri-miRNA. Then, they are cleaved by Drosha into a pre-miRNA. The pre-miRNA is exported from the nucleus to the cytoplasm by exportin 5. Then, it is processed by Dicer into a miRNA duplex to be later loaded into the Argonaute, which mediates the assembly of the RISC. The passenger strand is removed, and the RISC-miRNA complex can induce gene silencing [34,35].

2.2. MicroRNA composition

A miRNA molecule is composed of distinct regions, each having a specific function(s) in pairing, specificity, and ensuring repression efficiency [43]. Therefore, the miRNA sequence can be sectioned into domains: 5'-end anchor (nt 1), seed region (nt 2-7), central domain (nt 9-12), 3´ supplementary region (nt 13-16) and 3'-end tail (nt 12-22) [43]. The seed region is the primary determinant of binding efficiency. However, other miRNA molecule regions contribute to target recognition and influence binding efficacy (Fig. 6).

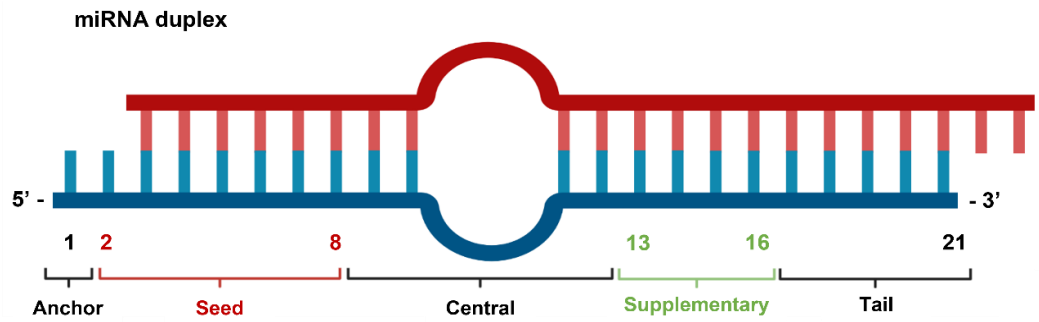

Figure 6 - Representation of the different regions that compose a functional miRNA molecule.

The 5'-end anchor is the first nucleotide in a miRNA molecule. Its primary function is enhancing miRNA targeting [43]. This nucleotide is often an adenosine, known as T1A which is recognised by the binding pocket of the Argonaute protein, ensuring the binding of the Argonaute protein to the respective miRNA [44].

The seed region is crucial in mRNA target recognition and specificity [45]. It is estimated that over 80% of miRNA's interaction with its target mRNA occurs via seed pairing [45]. The seed region comprises nucleotides 2 to 8 of the 5'-end of the miRNA and promotes the binding to the target mRNA. Thus, this region must be conserved to retain its specificity and downregulation capability [37–39]. However, the seed region's 6-7 contiguous nucleotides can appear more than once in the target's mRNA. Thus, to ensure complete target specificity, other domains present in the miRNA improve the targeting effectiveness [46].

The central region of the miRNA has a crucial role in efficient cleavage [46]. Nucleotides 9-11 can acquire a bridge conformation which generates a loop between nucleotides 1-5. Thus, the seed and supplementary regions are brought closer together [46]. This proximity enhances the affinity between the miRNA and target mRNA, it increases the specificity and downregulation efficiency. Furthermore, mismatches in this domain have been correlated with the incapacity of the RISC complex to form a functional catalytic conformation [43].

Nucleotides 13-16 from the supplementary region can also base pair with the target mRNA, as occurs with the seed region [46]. This complementarity arises mainly through Watson-Crick pairing without discontinuities. It has been demonstrated that base pairing with the supplementary region can compensate for imperfect seed pairing [47]. Thus, this binding can decrease the dissociation rate of the RISC and increase repression efficiency [47].

Furthermore, the binding of the Argonaute protein to the respective miRNA induces a conformational change of the protein that permits full seed region pairing and supplementary region exposure [44]. Therefore, these conformational changes enhance the pairing of the miRNA, which outcompetes other miRNAs with only the seed region available for binding [44].

The miRNA 3'-end tail composed of nucleotides 17-21 has also been shown to influence miRNA interaction with target mRNA and participate in mRNA degradation [46]. The 3'-end tail length

extension increases the interaction's stability in the miRNA's supplementary region. Furthermore, expanding this domain allows a higher number of nucleotides for target recognition [46].

2.3. MiRNAs target recognition and selectivity

In silico studies have shown that over 75% of human miRNAs exhibit secondary structures [48]. The miRNA secondary structure can increase molecule stability and shield it against nuclease degradation. Furthermore, a conformation with a lower Gibbs free energy is generally more stable. Thus, a miRNA can increase its half-life by re-shaping into a more stable secondary structure [48].

However, a change in miRNA conformation can also hide the seed region [48]. Likewise, mRNAs can also present secondary structures that make the miRNA binding site inaccessible. For binding to occur, the secondary structure needs to be dismantled. However, secondary structure dismantling only happens if the energy gained by miRNA-mRNA pairing surpasses the energy expended to break down the mRNA secondary structure. If this does not occur, the mRNA will remain with its secondary structure and unreachable binding site. As such, hidden seed regions or inaccessible binding sites limit the miRNA-mRNA pairing and reduce the degree of regulation of a given miRNA, leading to a slower silencing efficiency [48].

Additionally, even when a specific miRNA binds to its target mRNA, the silencing effect further depends on the hybridisation thermodynamics [49]. Accordingly, the lower the free energy of the miRNA-mRNA duplex is, the stronger the interaction will be, leading to a more efficient miRNA silencing over its target gene [50]. Additionally, the number of target sites within the mRNA sequence also dictates miRNA downregulation efficiency. Multiple target sites should be distanced for optimal repression by 10 to 50 nucleotides. Shortening distances lead to miRNAs' competition, which decreases their downregulation efficiency [50]. As such, one miRNA can distinctively regulate the expression of several mRNAs with unequal effectiveness, depending on some inherent characteristics of both molecules.

2.4. MicroRNA regulatory mechanism

The correct assembly of the RISC complex is vital for a miRNA to execute its biological function properly. After miRNA loading, the guide strand is separated from passenger strand [51]. Two factors modulate the choice of the guide strand from the miRNA duplex. The human Argonaute protein preferentially selects the guide strand with a uracil nucleotide at the 5'-end [52]. In addition, a lower relative thermodynamic stability also promotes the guide strand selection [51,53].

After guide strand selection and complete assembly of the RISC complex, the silencing mechanism can be initiated. Overall, there are two distinct silencing mechanisms: translational repression and target mRNA degradation [54,55]. The mechanism that occurs depends on the degree of complementarity between the target mRNA and the effector miRNA. For instance, if there is full complementarity and the Argonaute is still bound to the miRNA, then the target mRNA will endure endonucleolytic cleavage and be degraded, [54,55] which is particularly common in plants [55]. In bilaterian animals, such as humans, miRNA repression does not require full complementarity

between the seed region and the binding site [31,55]. This regulation model inhibits the translation process of the target mRNA through a complex enzymatic process that impedes the binding between the ribosome and the target mRNA [56]. Thus, both processes are viable for mRNA repression, differing mainly by the complementary extent and origin organism. Nevertheless, miRNAs, such as *miR-34a*, can modulate the expression of different target genes via both mechanisms [57] even with a transparent bias toward translation repression [57].

3. miR-34a

3.1. *miR-34a* as therapeutics for liver-associated diseases

As of 2016, approximately 700 mRNA targets had been identified for *miR-34a* [58]. From this list, it is possible to identify genes implicated in numerous biological functions, including proliferation, apoptosis, senescence, cancer stem-like cell phenotype, motility, and cell invasion. For instance, *miRNA-34a* can regulate carcinogenesis by repressing cell-cycle progress and apoptosis induction. Currently, several studies are being developed to restructure *miR-34a* expression in tumour cells. This could be exploited as therapeutics in cancer development [59].

More specifically, *miR-34a* is involved in various liver pathogenesis. Hence, it is essential to analyse how this miRNA can be exploited as a biomarker for certain diseases and used as a therapeutic target.

miR-34a tends to be downregulated in human liver cancers, including hepatocellular carcinoma (HCC) [60]. HCC is the most common type of liver cancer, exceeding all other types of cancer in terms of mortality in developing countries and ranks sixth in developed countries [60,61]. Ectopic expression of *miR-34a* can revert HCC development by suppressing tumour proliferation and invasion. As *miR-34a* expression is significantly impaired in HCC cell lines and patients, this miRNA has a strong potential as a therapeutic target for hepatic cancers [60].

Furthermore, *miR-34a* is a biomarker prognostic and staging of non-alcoholic fatty liver disease (NAFLD) [62]. This hepatic disorder is characterised by lipid accumulation in the liver. If not treated in time, this disease can worsen into non-alcoholic steatohepatitis (NASH), leading to fibrosis. NASH can progress into cirrhosis and then into HCC. Deletion of hepatocyte-specific *miR-34a* can diminish NAFLD progression. This miRNA can aggravate NAFLD progression into NASH by increasing lipid absorption, lipogenesis, apoptosis, and inflammation while hindering fatty acid oxidation therefore, *miR-34a* is a potential therapeutic target in treating NAFLD [62].

3.2. *miR-34a* targets genes expressed during liver development

Liver development is driven by the successive activation and repression of a complex gene network. In particular, *miR-34a* regulates the expression of several genes that ensure proper liver development, such as *Hnf4α* and *Notch2.*

3.2.1 Notch2

miR-34a directly targets the expression of *Notch2* by recognising its binding site in the 3'UTR region of this gene (Fig. 7). *Notch2* plays a significant role in cholangiocarcinoma development in human patients [63]. Thus, using an intermediary, such as *miR-34a*, to correct the improper expression of this gene may represent a therapeutic procedure for some liver diseases, such as NAFLD. Therefore, *miR-34a* behaves as o tumour-suppressive agent that can silence the expression of *Notch2* and prevent human cholangiocarcinoma progression. Thus, the exogenous delivery of this miRNA could be potentially used as therapeutics for hepatic diseases, as is the case for cholangiocarcinoma [63].

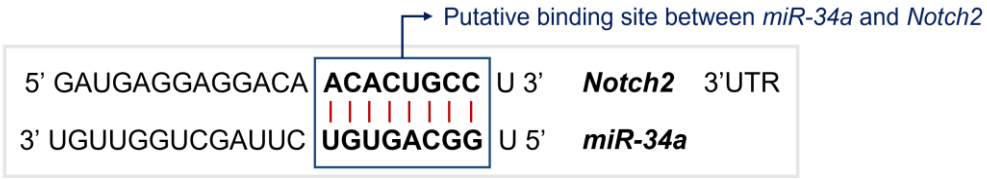

Figure 7 – Putative binding site for *miR-34a* and *Notch2* in the 3' UTR region in bold. Adapted from Kwon, H. et al. Epigenetic Silencing of miRNA-34a in Human Cholangiocarcinoma via EZH2 and DNA Methylation: Impact on Regulation of Notch Pathway. American Journal of Pathology 187, 2288–2299 (2017).

3.2.2. *Hnf4α*

Hnf4α is an essential transcription factor whose expression influences parenchyma morphogenesis mainly by regulating hepatocyte differentiation [18]. As a result, deregulation of *Hnf4α* expression hinders normal liver development [64] and cause pathogenesis [17]. Thus, abnormal expression of *Hnf4α* leads to atypical liver morphology with acute injuries [19].

Studies have demonstrated that *miR-34a* regulates *Hnf4α* [65]. There are three putative binding sites for *miR-34a* in the 3'UTR *Hnf4α* gene (Fig. 8) [65]. This regulation occurs mainly via translation inhibition, decreasing downstream gene expression.

However, when *miR-34a* is improperly expressed the downregulation over *Hnf4α* can lead to development of hepatic diseases [66]. For example, in NASH patients, *miR-34a* expression levels are often elevated, resulting in the downregulation of up to 80% of *Hnf4α,* which augments disease progression. Likewise, increased downregulation over *Hnf4α* in hepatocytes causes NAFLD development by inhibiting lipoprotein metabolism [66]. Additionally, in some liver diseases such as HCC, *Hnf4α* has found to be upregulated. That would make *miR-34a* an interesting tool to downregulate *Hnf4α* levels and prevent tumorigenesis [67].

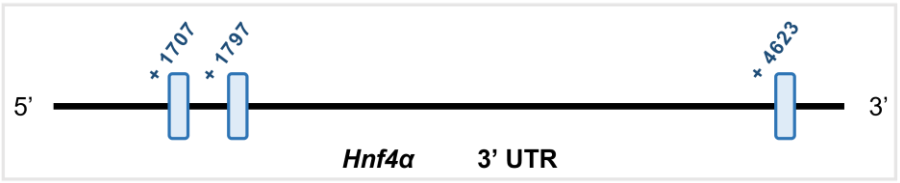

Figure 8 - Putative binding sites for *miR-34a* and *Hnf4α* in the 3' UTR region marked as blue rectangles. Adapted from: Salloum-Asfar, S., Arroyo, A. B., Teruel-Montoya, R., García-Barberá, N., Roldán, V., Vicente, V., Martínez, C., & González-Conejero, R. (2016). MiRNA-based regulation of hemostatic factors through hepatic nuclear factor-4 alpha. PLoS ONE, 11(5).

4. Delivery of chemically modified miRNAs

The first nucleic acid delivery system dates back to 1990 when naked exogenous mRNA was intramuscularly administered to mice [68]. However, this transfection process endured several difficulties. Since 1980 [69] lipidic-based delivery systems have been continuously developed to better cope with transport difficulties. Lipid nanoparticles (LNPs) are currently the most advanced system to deliver nucleic acids to the target cells and various diseases such as COVID-19 [70]. The use of LNPs for the targeted delivery of miRNAs aims to tackle two common challenges: target specificity and endosomal escape [71].

LNPs are often formulated with a helper lipid, a PEGylated lipid, an ionisable lipid, and cholesterol [72]. The helper lipid and cholesterol are essential in maintaining structural integrity. Furthermore, they also influence endosomal escape [73]. Onpattro was the first prescription medicine approved by the FDA, which exploits LNPs to deliver siRNA into hepatocytes [74]. This work showed that in loaded LNP, a portion of the helper lipid DSPC and cholesterol transition from the exterior to the interior of the nanoparticle, which is vital in stabilising the encapsulation of RNA [74].

The PEG-lipid also plays a vital role in the effectiveness of the LNP. This lipid is composed of a hydrophobic lipid directed to the particle's interior and a hydrophilic PEG-polymer facing the exterior of the particle. This lipid is frequently used to determine the size of the LNP. The concentration of the PEG-lipid is tightly controlled since PEG can interfere with the internalisation of the particle and impedes fusion during endosomal escape [73].

The ionisable lipid at low pH will acquire a positive charge. The positively charged LNP will interact with the negatively charged lipids in the inner leaflet of the endosome. As such, the cationic and anionic lipids will form an ion pair and change their conformation into a cone which will lead to the formation of the non-bilayer structure such as the inverted hexagonal H_{II} phase (Fig. 9). This type of conformation is not supported in the bilayer structure which leads to membrane disruption and miRNA release [75,76]. Therefore, the miRNA will be able to escape the endosomes and be dispersed in the cytosol for targeted gene silencing. As such, the charge at endosomal pH will infer its endosomal escape potential [75].

LNPs have already successfully delivered a hepatic-specific tumour suppressor miRNA decreasing hepatocellular carcinoma tumour growth by 50% even after 30 days [77]. However, after successfully delivery, miRNAs still need to survive in the intracellular environment of the target cell. As such, naked miRNA faces augmented obstacles that decrease its lifespan and downregulation efficiency. These challenges include degradation by RNases and off-target effects. A methodology used to reduce these effects is chemically modifying the miRNA molecules [78]. Common chemical modifications include methylations and the substitution of carbon for a nitrogen inside the ring system. Furthermore, base modifications can thermally destabilise the formation of duplexes, preventing an off-target effect. It is also feasible to replace the hydroxyl group on the C2 position to protect the molecule against nuclease degradation. This can be done, for instance, by the addition of amines or phosphates. Additionally, a molecule's backbone can also be chemically modified. For example, adding a phosphorothioate bond replaces the oxygen in the phosphate group with sulphur which prevents phosphatase degradation [78]. Therefore, the future of miRNA delivery relies on optimising its intracellular survival and activity effectiveness. That is the main reason that determining the most adequate miRNA chemical modifications would be a breakthrough in nucleic acid engineering and make a significant difference in upcoming studies.

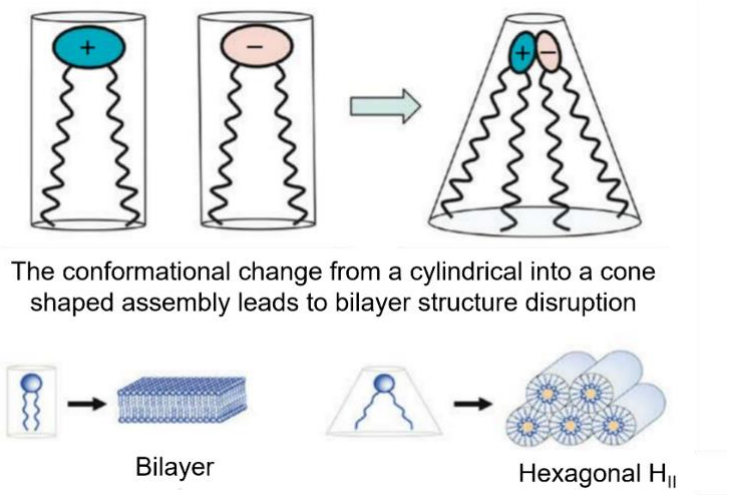

Figure 9 - The positively charged LNPs will form an ion pair with the negatively charged lipids in the inner leaflet of the endosome. This will change the normal cylindrical phospholipid organization into a coned shaped structure. The bilayer will shift to a hexagonal conformational which leads to its disruption. Adapted from: Semple, S. C. et al. Rational design of cationic lipids for siRNA delivery. Nature Biotechnology 28, 172–176 (2010).

Aim of the thesis

A global estimate of 2 million deaths is caused by liver diseases yearly [79,80]. Cirrhosis and liver carcinogenesis together account for 3.5% of worldwide mortality [79,80]. Excessive alcohol consumption plus the uncontrolled increment in obesity are leading causes of hepatic pathogenesis [79,80]. Furthermore, abnormal liver gene expression during embryonic development leads to severe hepatic disorders, resulting in early child mortality [80]. For example, Alagille Syndrome is an autosomal dominant disease characterised by bile duct paucity that affects distinct organs. Mutations in the Notch signalling pathway predominantly cause this disease, ultimately leading to acute cholestasis even during infancy. Unfortunately, there is still no cure for ALGS or numerous other embryonic defects [80].

Hence, the innovative strategy to surpass ongoing health problems is to exploit pioneering technologies and modulate them into cutting-edge therapeutics. One plausible starting point are miRNAs. These molecules can regulate the expression of a large subset of target genes involved in the most diverse biological functions. They have the therapeutic potential to restore normal gene expression deregulated due to an embryonic defect or during pathogenesis.

Despite the undeniable potential of miRNAs as therapeutics, there are still challenges that need to be outdone. These include a shortage of efficient delivery vehicles and elevated intracellular degradation. As such, extra and intracellular barriers often limit the efficiency of nucleic acids delivery systems. However, LNPs have been demonstrated to be excellent nucleic acid delivery mechanisms in various diseases such as COVID-19 [70]. Due to their impressive endosomal escape capability and outstanding delivery efficiency, they have the potential to become a tool that will reform nucleic acid therapeutics. Furthermore, to overcome cytoplasmic degradation, many efforts are being made to develop innovative miRNA chemical modifications to increase stability within a cell. This would lead to a prolonged intracellular persistence resulting in increased activity time.

This study aims to use chemically modified miRNA to modulate the expression of target genes which play a pivotal role in hepatic development and pathogenesis. As such, *miR-34a*, a critical regulatory molecule in several hepatic functions, will be used to study how the downregulation of its target genes, *Notch2* and *Hnf4α*, will modulate hepatic specification. *miR-34a* modified variants will be encapsulated with LNPs and this complex will be administered in isolated mouse E13.5 hepatoblasts. This embryonic stage marks the ideal time to study the hepatic embryogenesis. Thus, this study will determine the optimal parameters for an effective *miR-34a* transfection with LNPs in liver progenitor cells. Furthermore, it will determine which chemical modifications are more suitable for *miR-34a* downregulation efficiency and intracellular survival. In future work, these findings can be employed to reverse and repair abnormal gene expression even during early embryonic development.

Materials and Methods

1. Ethical statements and animal handling

Animal experiments were performed with the approval of the Regional Animal Research Ethical Board of Stockholm, Sweden. Animal handling and embryo collection were conducted according to EU legislation's ethical permit 2987-2020. During the experiments, mice were kept in a pathogen-free environment at 22˚C ambient temperature in Wallenberg laboratory (KM-W) at Karolinska Institutet. The animals lived under a 12h light/dark cycle with free access to food and water. The study was conducted on CD1 mice strain at embryonic day 13.5 (E13.5).

High genetic variability makes these mice less prone to genetic defects, which is suitable for gene expression studies. At embryonic day 13.5, pregnant female mice were euthanised in a closed cage with a CO_2 atmosphere followed by cervical dislocation. Upon animal sacrifice, the uterus was collected and stored in cold PBS for subsequent liver dissection.

2. Liver collection and hepatoblast isolation

The E13.5 embryos were dissected under the stereomicroscope (Leica) in cold PBS with appropriate dissection utensils. Then the livers were removed, transferred to cold PBS and broken down by pipetting up and down. The liver solution was then dissociated in liver perfusion medium (Gibco) for 20 minutes at 37˚C, mixing every 5 minutes. The samples were further digested with liver digestion medium (Gibco) for 20 minutes at 37˚C with mixing by pipetting every 5 minutes. Afterwards, the cell suspension was drained in a cell strainer. The erythrocytes were lysed with red blood cell lysis buffer (155 nM NH_4Cl, 10 nM $KHCO_3$, and 0.1 mM EDTA, pH 7.4) for 5 minutes on ice. Afterwards, hepatocyte differentiation medium (5% Fetal Bovine Serum [FBS], 1X L-Glutamine, 1X non-essential amino acids in DMEM High Glucose medium) was added to the solution. The number of cells was then counted on a Countess II Automated Cell Counter (Life Technologies). For each experiment, around 24-26 embryonic livers were collected, resulting in an average of $3.50x10^6$ to $5.50x10^6$ cells.

Hepatoblast isolation was performed via magnetic-activated cell sorting (MACS). This technique uses magnetic beads coated with antibodies specific to a cell surface marker [73]. At E13.5, hepatoblasts highly express DLK1. Thus, it was possible to isolate hepatoblasts using beads covered with antibodies that specifically bind to DLK1 [81].

Briefly, the cell suspension was firstly incubated with the blocking antibody Rat Anti-Mouse CD16/CD32 (BD Biosciences, 1:100) for 10 minutes on ice. Immediately after, the cells were incubated for 15 minutes on ice with anti-Dlk1-FITC (Nordic Biosite) at 1:40. Then, the samples were washed twice with washing buffer (0.5% BSA and 2 mM EDTA in PBS). The cells were resuspended in 150 ml of buffer, and 15 µl of anti-FITC microbeads (Miltenyi Biotec) were added to the solution for 15 minutes on ice. Subsequently, the column for magnetic cell sorting was prepared. The column was placed on a permanent magnetic block and equilibrated with MACS buffer (0.5% BSA and 2 mM EDTA in PBS). Afterwards, the cell solution was loaded, and the DLK1-expressing hepatoblasts remained in the column due to the attraction between the

magnetic beads and the magnetic block. The column was washed three times with MACS buffer to remove DLK1 negative cells. The final step was to elute the hepatoblasts with pressure from the column onto a 15 ml falcon tube using a syringe loaded with MACS buffer. Thus, as the cells migrate through the column, the cells attached to the magnetic beads were retained in the column until subsequent elution [82]. After that, the eluate was recovered in a 1.5 microcentrifuge.

3. Lipid nanoparticle formulation and *miR-34a* variants

Following hepatoblast isolation, cells were ready for seeding and transfection. Lipid nanoparticles were used to deliver the chemically modified variants of *miR-34a* to the isolated hepatoblasts. The LNPs were constructed with four complementing elements: an ionisable lipid (C12-200), a helper lipid (DSPC), cholesterol, and a PEGylated lipid (Fig. 10) [83].

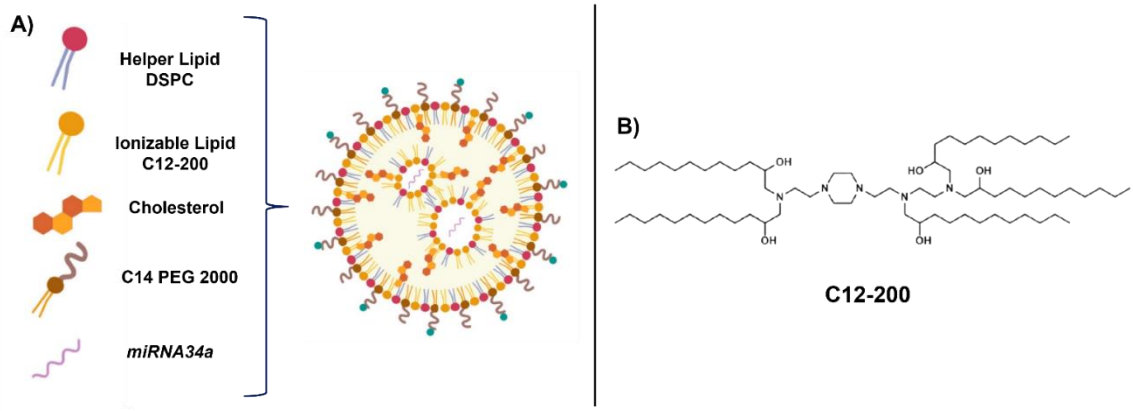

Figure 10 - A) Representation of the Lipid nanoparticles components. B) Molecular structure of the ionisable lipid C12-200. Adapted from: Swingle, K. L., Hamilton, A. G. & Mitchell, M. J. Lipid Nanoparticle-Mediated Delivery of mRNA Therapeutics and Vaccines. Trends in Molecular Medicine 27, 616–617 (2021) [70].

Seven *miR-34a* variants with different chemical modifications were designed and tested. The chemical modifications include 5'-end phosphorylation (5'-PHOS), insertion of a 5´-end vinyl phosphate group at the C1 position and substitution of phosphodiester (PO) bonds with phosphorothioate (PS) bonds at the 5' and 3'-ends of the molecule. The sequences of each *miR-34a* variant (1-7) can be seen in Table 1. The hepatoblasts were also transfected with a miR scramble (scr-LNP) control as a negative control. A scrambled control is defined as a random reorganisation of the nucleotides that compose a particular miRNA into a new and inactive molecule.

Table 1 – Sequences of each *miR-34a* variant transfected with LNP. Phosphorylations at the 5'-end are marked in red as "PHOS", the substitution of PO by PS is exemplified in blue as "s", and the addition of a 5'-end vinyl phosphonate group is represented in green as "VINYL-P".

***miRNA-34a* variants**	**Sequence**
miR-34a 1	UGGCAGUGUCUUAGCUGGUUGU
miR-34a 2	**PHOS**-UGGCAGUGUCUUAGCUGGUUGU
miR-34a 3	**PHOS**-U**s**GGCAGUGUCUUAGCUGGUUGU
miR-34a 4	**PHOS**-U**s**GGCAGUGUCUUAGCUGGUUG**s**U
miR-34 5	**PHOS**-U**s**G**s**GCAGUGUCUUAGCUGGUU**s**G**s**U
miR-34a 6	**PHOS**-**s**U**s**G**s**GCAGUGUCUUAGCUGGUU**s**G**s**U
miR-34a 7	(**VINYL-P**)-U**s**G**s**GCAGUGUCUUAGCUGGUU**s**G**s**U
scr *miR-34a*	GUUAGUGAUACGAUGAUAAA

4. Cell culture and transfection

Before the seeding, the 96-well plates were coated with 10 µg/ml of fibronectin (Merck) diluted in PBS and incubated at 37˚C for 30 minutes. Afterwards, the cells were seeded in two types of growth medium: non-differentiation and differentiation, depending on the experiment. The non-differentiation medium was supplemented with Tanimizus' media (10% Fetal Bovine Serum, 1x ITS-X, 0.1 µM Dexamethasone, 10 nM Nicotinamide, 10 ng/ml HGF, 10 ng/ml EGF in DMEM/F-12, GlutaMAX supplement [Sigma-Aldrich]). Cell seeding densities between 30 000 and 45 000 cells/well were tested, from which 35 000 cells/well was found to be the optimal cell density for seeding E13.5 hepatoblasts.

For hepatoblast differentiation, the cells were diluted in differentiation media (5% FBS, 2 mM L-glutamine, 1x ITS-X, 0.1 µM Dexamethasone in Helin´s MCDB131 media with glutamine [Thermo Fisher Scientific]). These cells were cultured in a sandwiched system composed of fibronectin as a layer on the bottom of the well and Matrigel on top of the seeded cells. Thus, after dilution, 4 vol/vol % Matrigel was added to the media with cells. For hepatoblast differentiation, cells were seeded with a cell density of 32 000 cells/well.

Shortly after seeding, the cells were transfected with seven *miR-34a*-LNPs and one scr-LNP to a final concentration of 100 nM and 100 µl of medium per well.

The cells were also transfected with double-stranded *miR-34a* (*miR-34a*-lipo), miR scrambled control (scr-lipo) and siRNA specific for *Hnf4α* (siRNA-*Hnf4α*-lipo, [Thermo Scientific™]) using Lipofectamine RNAiMAX (Thermo Scientific™). Briefly, lipofectamine was diluted in OPTIMEM medium at a ratio of 25:1.5 vol/vol of OPTIMEM:lipofectamine. Afterwards, *miR-34a,* scr-lipo, or siRNA-*Hnf4α*-lipo (each final concentration of 100 nM) were added to the complexed lipofectamine solution at a ratio of 1:1000. The solution was incubated for 5 minutes at RT. Then the transfection solution was added to the cells diluted in the culture medium.

All the transfections were done in triplicates. Cells were cultured in standard conditions of 37˚C, 5% CO_2 and 95% humidity for 12h, 24h, 48h (non-differentiating medium), and 72h (differentiating medium).

5. RNA isolation

After the adequate culture time, the cells were collected, and the RNA was isolated with the *miR*vana™ miRNA Isolation kit (Thermo Scientific™), according to the manufacturer's protocol. Succinctly, the wells were firstly washed with cold PBS, followed by the addition of 100 µl of Lysis/Binding buffer. Afterwards, 1/10 volume of miRNA Homogenate Additive was supplied to the cell lysate, then mixed and incubated on ice for 10 minutes. Subsequently, 300 µl of Acid-phenol chloroform was added, and the samples were vortexed for 1 minute and centrifuged for 5 minutes at maximum speed. To the supernatant 1.25x volume of 99%, ethanol was added, and the solution was transferred to a filter cartridge and centrifuged for 15 seconds at 10 000 rpm. The flowthrough was discarded, and the column was washed once with 700 µl of the first washing solution, followed by 10-second centrifugation at 10 000 rpm. Then, the column was washed twice with the second washing solution. For the second washing step, the column was centrifuged for 10 seconds at 10 000 rpm, while for the third washing step, the column was centrifuged for 1 minute at 10 000 rpm. RNA was eluted from the column with the 50 µl of pre-heated elution buffer and centrifuged for 30 seconds at maximum speed. After RNA isolation, the RNA concentration and purity were measured with Nanodrop 2000 (Thermo Fisher Scientific).

Following RNA isolation, the samples were treated with DNase to eliminate residual DNA contamination. Two different DNase treatments were used to determine the most efficient one and ensure RNA purity. The first treatment was performed with the DNA-free™ DNA Removal kit (Thermo Scientific™). For this treatment, the RNA was firstly diluted to 200 ng/µl. Then, 0.1 volume of 10X DNase I buffer and 1 µl of rDNase I was added and mixed with the RNA solution. The enzyme was incubated with the RNA at 37˚C for 20-30 minutes. Protein deactivation occurred by adding 0.1 volume of DNase inactivation reagent and incubating for 2 minutes at RT. The solution was centrifuged at 10 000xg for 1.5 minutes, and the RNA was collected in the supernatant. The second DNase treatment used was DNase I, Amplification Grade (Thermo Scientific™). For this treatment, 1 µg of RNA, 1 µl of 10X DNase I Reaction buffer and 1 µl of DNase Amp Grade were added to the solution. The solution was incubated at room temperature (RT) for 15 minutes. Then, the enzyme was deactivated by adding 1 µl of 25 mM EDTA and incubating for 10 minutes at 65˚C. After both DNase treatments, the RNA concentration and purity were measured again with Nanodrop.

To assess the purity level of isolated RNA, the absorbance values of three wavelengths, 230, 260 and 280 nm, are to be considered. To establish an RNA sample as pure, the ratio value for A_{260}/A_{280} should be 2.0, while for ratio A_{260}/A_{230}, the value should be between 2.0-2.2. Abnormal results may indicate contamination from proteins or reagents used during RNA isolation, such as phenol. However, when the RNA concentration is lower than 10 ng/µg, the result from the

Nanodrop measurement is not trustworthy since the RNA's concentration is below the equipment's sensitivity [84].

6. Primer Design

Primers for *Notch2*, *Hnf4α*, *Sox9* and *Gapdh* were designed (Table 2 in the Annexes). The primer pairs were constructed to have a melting temperature of around 60˚C, GC content of 57-63% and designed to amplify the product size between 150-250 bp. In addition, each primer pair was devised to prevent hairpin formation and self-dimerization. Furthermore, an NCBI blast was performed on each primer to predict and avoid off-target binding. To evaluate primer quality in terms of specificity and efficiency, a temperature gradient PCR followed by electrophoresis was achieved. The PCR was performed with (2x) DreamTaq Green PCR Master Mix (Thermo Scientific™). Each PCR tube contained 50 µl of the reaction mix composed of 2x DreamTaq Green master mix, 50 ng of cDNA (on the non-transfected sample), 1 µM forward and reverse primer and water. The thermal cycler was set up as follows: initial denaturation at 95˚C for 1 minute. Then 30 cycles of denaturation at 95˚C for 30 seconds, annealing at 58-63˚C for 30 seconds, extension at 72˚C for 1 minute and a final extension at 72˚C for 5 minutes. After the PCR, 25 µl of each sample were put on a 1% agarose gel mixed with 10 µl of GelRed® Nucleic Acid Gel Stain (Biorad) prepared in TAE buffer (0.4 M tris acetate pH 8.3 and 0.01 M EDTA in ultrapure water).

7. cDNA synthesis

cDNA synthesis for miRNA was performed using TaqMan™ MicroRNA Reverse Transcription Kit (Applied Biosystems™) and TaqMan probes specifically binding to *sno202*, *sno234* and *miR-34a.* For miRNA reverse transcription, each reaction tube contained 10 ng of RNA. The reaction final volume was composed of 1 mM dNTPs, 50 U MultiScribe Reverse Transcriptase, 10x Reverse transcription buffer, 4 U RNase inhibitor, 5x RT primer and 8.25 µl of RNase-free water to a final volume of 15 µl in each reaction tube. The cDNA was amplified in a thermal cycler in three consecutive steps. First, the annealing for 30 minutes at 16˚C, followed by an extension for 30 minutes at 42˚C and enzyme inactivation at 85˚C for 5 minutes.

cDNA synthesis for mRNA was done with Maxima First Strand cDNA Synthesis Kit for RT-qPCR (Thermo Scientific™). RNA was firstly diluted to 100 ng/µl. Each reaction tube comprised 5x Reaction Mix, 400 U of Maxima Enzyme Mix, 500 ng of RNA and 9 µl of nuclease-free water to a final volume of 20 µl in each reaction tube. The thermal cycler was also programmed for cDNA synthesis in three steps:annealing for 10 minutes at 25˚C, amplification for 15 minutes at 50˚C and enzyme denaturation at 85˚C for 5 minutes.

8. Quantitative PCR (qPCR)

For miRNA qPCR TaqMan™ Universal Master Mix II, no UNG (Applied Biossystems™) was used. The cDNA solution was first diluted to 0.165 ng/µl. Then, in each reaction tube, 20x of TaqMan miRNA assay TM primers, 2x TaqMan Universal PCR Master Mix, no UGN, 0.858 ng of cDNA and 7.67 µl of nuclease-free water were added to a final volume of 20 µl. The qPCR was set up

for 40 cycles as follows: hold for 10 minutes at 95˚C, denaturation for 10 minutes at 95˚C, annealing and extension for 60 seconds at 60˚C.

The Fast SYBR™ Green Master Mix (Applied Biosystems™) was used for mRNA qPCR. Each reaction tube contained 2X Fast SYBR Green Mix, 0.71 M of forward and reverse primer, 10 ng of cDNA and 1 µl of RNase-free water to a final volume of 15 µl. The qPCR thermal-cycling conditions were set up for an initial hold for 20 seconds at 95˚C, followed by 40 cycles of denaturation for 3 seconds at 95˚C and annealing/extension for 30 seconds at 60˚C.

Reactions for qPCR were executed with three technical replicates. For each well, qPCR results were given as the cycle threshold (C_T) number. A non-template control (NTC) was also performed as a negative control in every qPCR plate. Relative gene expression was normalised with standard qPCR calculations. The first step was calculating the average of the results obtained for the triplicates of each sample. A simple average calculation is enough for the gene of interest (GOI), *miR-34a*, because there is only one data set per sample. In contrast, for the two reference genes (RG), a geometric average is needed since, for each sample, the final result has to include the average of both *sno202* and *sno234*. Each sample's relative gene expression (RQ) values were then estimated through Equation 1. Succinctly, considering a primer efficiency of 100%, the RQ value is determined by calculating 2 to the power of the difference between the calculated average C_T value of the GOI and the geometric average of the RG. The samples were normalised with the control of the non-transfected (NT) cell to normalise the obtained results fully. This was performed by dividing the estimated RQ value of each sample by the RQ value of NT cells.

$$\mathrm{RQ} = 2^{-(\text{average CT GOI} - \text{geometric average CT RG})} \quad \text{(Eq. 1)}$$

9. Protein isolation

The cells were washed once with cold PBS and then collected with 30 µl of RIPA Lysis and Extraction Buffer (Thermo Scientific™) with cOmplete™, EDTA-free Protease Inhibitor Cocktail (Roche). The samples were then centrifuged at 14 000xg at 4˚C for 15 minutes, and the supernatant was transferred to a new 1.5 ml tube and stored at -80˚C until usage. The protein concentration was assessed with the colourimetric Pierce 660-nm Protein Assay kit (Thermo Scientific™). The protein standards 125 to 2000 µg/ml were used, and each standard and protein sample was mixed with Protein Assay Reagent at a ratio of 1:15. After 5 minutes of incubation at RT, the protein concentrations were read on a VersaMAx Microplate reader (Molecular Devices). A Concentration curve was prepared to determine the concentration of each sample.

10. SDS-PAGE and Western blot

The sodium dodecyl sulfate-polyacrylamide gel electrophoresis (SDS-PAGE) was prepared using the Mini-PROTEAN® TGXTM Precast Gel (BioRad) and the BioRad gel electrophoresis system. Each protein sample was mixed with 2x Laemmli buffer (Biorad) and DTT to a final concentration of 100 mM. The samples were then denatured for 3 minutes at 80˚C and loaded on the gel; 3 µl of Precision Plus Protein Dual Color Standards (Bio-Rad) was used as a protein marker. The

electrophoresis runs for 1-2h at 100V in 1X Running Buffer (25 mM Tris, 190 mM glycine, 0.1% methanol).

The 0.45 µM Immun-Blot PVDF Membrane (BioRad) was used for protein wet transfer from the gel. Initially, the membrane was activated with 100% methanol for 10 seconds, then washed with water and 1x Transfer buffer (25 mM Tris, 190 mM Glycine, 20% methanol). The transfer was conducted in 1x Transfer buffer at 4˚C for 1h, at 100V.

After transfer, the membrane was washed with tap water once and then blocked with 5% skim milk prepared in 10 ml 1x Tris-buffered saline solution with 0.1% Tween® 20 Detergent (TBST) buffer (0.1% Tween, 900 ml dH_20 with 100 ml of 10x TBS (24 g Tris, 88 g NaCl, 900 ml dH_2O, pH 7.6) for 30min-1h at RT on a rocker. The membrane was then washed in 1x TBST for 10 minutes at RT. The primary anti-goat *Hnf4α* antibody (Santa Cruz) was diluted at 1:600 in TBST to a final volume of 10 ml and incubated overnight at 4˚C on a rocker. Next, the membrane was washed three times for 5-10 minutes with TBST. The secondary antibody was prepared to a final volume of 10 ml at a dilution of 1:10 000 anti-rabbit HRP in 5% skimmed milk and incubated with the membrane for 1h at RT. Then the membrane was washed four times with 1X TBST for 10 minutes. The developing solution was prepared by mixing clarity western peroxide reagent and clarity western luminol/enhancer reagent at a 1:1 ratio from the Clarity™ Western ECL Substrate (Bio-Rad) kit. The membrane with the developing mix was placed on the Biorad Gel Doc XR+ Imaging System (Bio-Rad) support. The samples were imaged from 0.5 to 300 seconds and analysed using ImageLab™ version 6.0.1 software.

11. Cell staining

The cells in 96 well plates were first washed with cold PBS and fixed with 4% Paraformaldehyde (Sigma) for 15 minutes at RT. Then the cells were washed with PBS permeabilised with 0.5% TritonX (Sigma) in PBS for 5 minutes at RT. After one wash with PBS, 50 µl of the blocking antibody (3% donkey serum in 0.1% TritonX in PBS solution) was added to the wells for 1h at RT. Cells were rewashed with PBS, and the primary antibody (1:800 Hnf4α Abcam antibody prepared in 0.1% TritonX in PBS 3% donkey serum) was added overnight at 4˚C. The cells were washed three times with PBS for 10 minutes at RT the next day. A solution of the secondary antibodies was prepared (Alexa fluor anti-rabbit 488 1:500 and DAPI 1:1000) and added to the cells for 1h at RT. The cells were then rewashed with PBS for 10 minutes at RT. For imaging, 100 µl of PBS was placed in each well. E13.5 hepatoblasts were imaged with a Zeiss LSM 900 Airyscan confocal microscope.

12. Statistical Analysis

The statistical calculations were performed with GraphPad Prism 8.0.1 (Dotmatics). The results were divided into two groups for the statistical analysis: the controls and the treatment samples. The control group includes non-transfected samples, and the scramble controls transfected both with LNPs and lipofectamine. The treatment samples group comprises the seven chemically distinct *miR-34a* variants transfected with LNPs, *miR-34a* transfected with lipofectamine, and

Hnf4α siRNA also transfected with lipofectamine. The statistical tests aimed to determine if there was a statistical difference between the two groups. The statistical analysis depends on the dualism between the null hypothesis (H_0) and the alternative hypothesis (H_1). H_0 proposes that there is no relationship between the variables. In contrast, H_1 states a relationship between the obtained results. To determine if the results have statistical significance, it is necessary to calculate the probability value (p-value). The p-value determines how rarely the results consider H_0 as true. Hence, the smaller the p-value, the higher probability of rejecting H_0. As a standard practice, the results were considered statistically significant only when the p-value was below 0.05 [85].

The control group and the treatment group come from the same experiments. The difference between them is the presence or absence of active *miR-34a*. The two groups have different variables that influence the observations. As such, the samples are independent, and thus an independent statistical test was used. Furthermore, the statistical test was set-up as one-tailed since the main aim in these experiments is to detect if the genes are differentially expressed between the control and the treatment samples. A one-tailed test rejects H_0 based on one side of the distribution curve tail. Thus, the control may only differ from the treatment samples by presenting either higher or lower values [85]. The difference can be either upregulation or downregulation. It does not require both up and downregulation. Therefore, a one-sided statistical test is suitable for the obtained results. H_1 states that the presence of *miR-34a* leads to a change in the expression of the target genes. In contrast, H_0 states no statistical significance between the controls and the treatment samples. To assess whether the results followed a non-parametric or normal distribution, it is valid to use the central limit theorem as standard procedure. Sample sizes equal to or above 30 can often be considered to follow a normal distribution [85]. However, a small number of biological replicates was obtained, hence is not accurate to assume that the variables have a normal distribution. Therefore, the attained results were treated with non-paramedic statistical tests [85,86]. Furthermore, the conducted experiments have between one and four biological replicates. Thus, a statistical test more adequate for a smaller sample size had to be used. Considering all these factors, the Mann-Whitney is the statistical test that better fits the attained results. As such, H_0 is rejected when the distributions from the two samples are not identical, caused either by up or downregulation.

Results

1. From E13.5 mice livers to RNA

Experiments were conducted in hepatoblasts isolated from E13.5 embryonic livers (Fig. 11). Liver development rapidly evolves after E8.5, from which hepatoblasts differentiate at the ventral foregut [6]. Liver progenitor cells behave as bipotent cells able to differentiate into the two main hepatic cell types. Thus, hepatoblasts are the most appropriate cells to analyse changes in gene expression during liver embryogenesis. At E13.5, hepatoblasts' differentiation into hepatocytes and cholangiocytes is already taking place. Thus, E13.5 hepatoblasts represent the optimal embryonic stage for studying early *Notch2* and *Hnf4α* expression.

Additionally, E13.5 hepatoblasts highly express DLK1. Thus, these cells were isolated with MACS using magnetic beads that bind to DLK1-positive cells. Hepatoblast isolation was sectioned into two experimental steps. Initially, livers endured perfusion, digestion, and red blood cell lysis. At this stage, a large amount of digested hepatic cells was attained. The second stage aimed to isolate DLK1-positive hepatoblasts using MACS. After isolation, around 3.50×10^6 and 5.50×10^6 hepatoblasts were recovered.

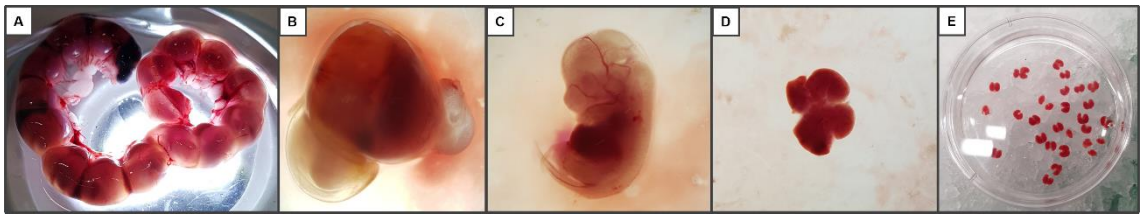

Figure 11 - Steps from uterus removal to embryo collection. A) CD1 strain uterus. B) Isolated embryo inside yolk sac. C) E13.5 mouse embryo (55x magnification). D) E13.5 mouse liver (55x magnification). E) Livers acquired for one experiment placed in cold PBS in a petri dish.

After hepatoblast isolation, the cells were seeded in 96-well plates with a cell density of 35 000 cells/well. To merely study the downregulation effect that *miR-34a* transfected with LNPs (*miR-34a*-LNP) had on target genes, hepatoblasts were cultured from 12 to 48h in the non-differentiation medium. To analyse the gene expression upon *miR-34a* transfection during hepatic differentiation, hepatoblasts were cultured for 72h in differentiation media.

After incubation with the *miR-34a*-LNP variants, hepatoblasts were collected, and the RNA was isolated. The concentration of the isolated RNA varied significantly among the different experiments. A higher amount of RNA was secluded in experiments where cells were cultured for extended periods since cells had more time to adapt and proliferate. In contrast, when cells were cultured for a shorter time, such as 12h, the amount of isolated RNA was significantly lower due to the lower number of cells. Furthermore, RNA isolated from cells transfected with *miR-34a*-lipo or siRNA-*Hnf4α*-lipo usually led to lower amounts of RNA. In contrast, non-transfected cells resulted in higher RNA yield.

Gene expression was assessed with RT-qPCR. As standard procedure, *sno202* and *sno234* were used for quantitative normalisation as internal controls of miRNA expression in mouse livers [87]. Therefore, cDNA synthesis was performed for miRNA, specifically for *sno202*, *sno234* and *miR-34a* and for total mRNA after RNA isolation.

2. *miR-34a*-LNPs successfully transfected hepatoblasts and downregulated target genes

miR-34a variants' transfection efficiency was assessed with RT-qPCR. Hence it was necessary first to establish the ideal time point between transfection and cell collection.

In the first conducted experiment, after transfection and seeding, cells were cultured in non-differentiating media for 12h. This starting point was carefully chosen since *Hnf4α* has a short half-life of 6h [88]. After 12h of cell culture, the cells were collected, and RNA was isolated. Then, RT-qPCR for miRNA and mRNA was performed. qPCR for miRNA was completed to assess the levels of *miR-34a* within the cells after 12h and to estimate transfection efficiency and intracellular persistence of the different *miR-34a*-LNPs. qPCR for mRNA was conducted to determine how gene expression varies upon 12h of *miR-34a*-LNPs transfection. The 12h time-point experiment was repeated twice in cells prevenient from different mice but under the same conditions to achieve two biological replicates.

To validate *miR-34a*-LNP transfection, miRs transfected with lipofectamine (miRs-lipo) were firstly assessed (Fig. 12A). Cells transfected with the negative control, scr-lipo, had a *miR-34a* median fold increase of only 0.10. Therefore, *miR-34a* expression remained close to the endogenous levels shown in the NT cells. A wild-type *miR-34a* was also transfected with lipofectamine (*miR-34a-lipo*). The *miR-34a*-lipo transfection led to a *miR-34a* median relative fold raise of 2716.69. To later validate *Hnf4α* downregulation, cells were additionally transfected with siRNA specific for *Hnf4α* with lipofectamine (siRNA-*Hnf4α*-lipo). The median relative level of *miR-34a* in cells transfected with siRNA-*Hnf4α*-lipo had a fold increase of 3.87 compared to the NT cells.

Following this, the transfection efficiency of the seven *miR-34a* variants transfected with LNP was analysed (Fig. 12B). To validate the transfection efficiency of the *miR-34a*-LNP, a negative scrambled control transfected with LNPs (scr-LNP) was administered to the cells. The scr-LNP had a small median fold increment of 1.48. This result suggests that the level of *miR-34a* was slightly higher than in the NT cells. Nevertheless, this increment is much lower than the expression values attained after transfection with the *miR-34a*-LNP. As such, transfection with scrambled *miR-34a* with either lipofectamine or LNPs leads to a minimal increase in *miR-34a* endogenous levels.

After 12h of culture time, variant 1 had the highest fold rise of 295.85. Surprisingly, variant 1 comprises only the naked nucleotide sequence of *miR-34a* without any chemical modification. Thus, this molecule is expected to be more susceptible to degradation by exonucleases. However, after 12h, there was no indication of enzyme degradation. Likewise, variant 4 presented the second-highest relative level fold surge of 262.84. This variant has a 5'-PHOS and one PS bond at the 5' and 3'-ends. Subsequently, the insertion of PS bonds protects the molecule from

exonuclease attacks at both ends, which increases intracellular survival after 12h. In contrast, the variant with the lowest transfection efficiency was variant 3, with a relative fold increment of 75.6. This molecule only has a PHOS and a PS bond at the 5'-end. Hence, a single PS bond at the 5'-end does not significantly improve transfection effectiveness or intracellular survival (Fig. 12B).

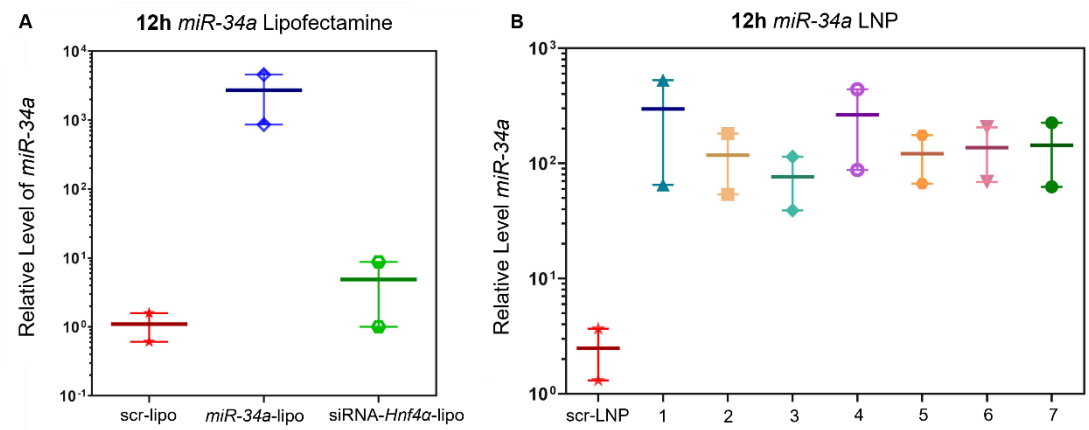

Figure 12 - RT-qPCR results of *miR-34a* relative expression after 12h of hepatoblasts transfection with two biological replicates. A) miRs transfected with lipofectamine: scrambled control (scr-lipo); *miR-34a* (*miR-34a*-lipo) and siRNA (siRNA-*Hnf4α*-lipo) transfected with RNAiMAX. B) Samples: scrambled control transfected with LNPs (scr-LNP); *miR-34a* 1, 2, 3, 4, 5, 6, 7 transfected with LNPs (*miR-34a*-LNP). Samples normalised to non-transfected cells set as 1.00. Statistical analysis was performed with the one-tailed Mann-Whitney statistical test.

After assessing *miR-34a* transfection efficiency, the downregulation of the target genes was measured. When hepatoblasts were transfected with scr-lipo, the expression of *Notch2* decreased slightly (Fig. 13A). However, transfection with scr-lipo had not increased *miR-34a* levels, as seen in Fig 12A. Thus, the small decrease in *Notch2* expression could result from intrinsic cellular adaptations to the culture media and conditions. On the contrary, the expression of *Notch2* in the cells transfected with *miR-34a-lipo* was expected to decrease substantially. However, *Notch2* relative level slightly increased to 2.80. Thus, *miR-34a* transfection with lipofectamine did not downregulate *Notch2* after 12h. Moreover, siRNA-*Hnf4α*-lipo transfection resulted in a *Notch2* decreased median expression level of 0.26. Hence, siRNA transfection might indirectly modulate *Notch2* expression, or siRNA, specific for *Hnf4α,* may have an off-target effect on *Notch2*.

In the next step, *Notch2* downregulation with *miR-34a*-LNP was analysed (Fig. 13B). Among all variants, variant 1 had the highest variability between the two biological replicates. Thus, variant 1's *Notch2* downregulation within 12h is quite unstable and more experiments had to be conducted to verify the results. This variability may result from the absence of chemical modifications making the molecule more susceptible to degradation. After 12h, variant 6 had the highest downregulation efficiency on *Notch2* (fold decrease of 0.50). This variant was designed with three PS bonds at the 5'-end and two at the 3'-end. After 12h, an increased number of PS

bonds seems to protect the molecule against degradation, causing an augmented activity. In contrast, variant 3 with only one PS bond at 5'-end had a much lower downregulation efficiency which is corroborated by its lower relative expression levels, possibly due to nuclease susceptibility.

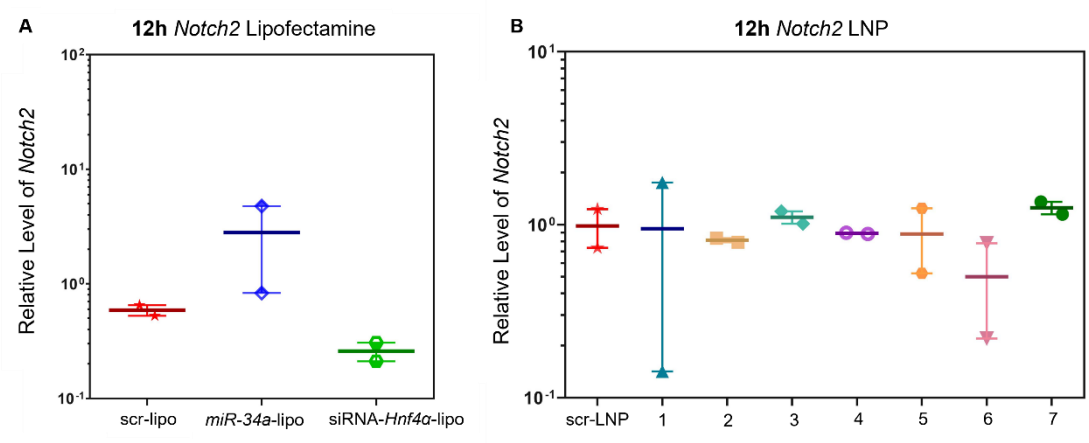

Figure 13 - RT-qPCR results of *Notch2* mRNA relative expression after 12h of transfection isolated E13.5 hepatoblasts with two biological replicates. A) miRs transfected with lipofectamine: scrambled control (scr-lipo); *miR-34a* (*miR-34a*-lipo) and siRNA (siRNA-*Hnf4α*-lipo) transfected with RNAiMAX. B) Samples: scrambled control transfected with LNPs (scr-LNP); *miR-34a* 1, 2, 3, 4, 5, 6, 7 transfected with LNPs (*miR-34a*-LNP). Samples normalised to non-transfected cells set as 1.00. Statistical analysis was performed with the one-tailed Mann-Whitney statistical test.

As for *Hnf4α*, both the transfection with *miR-34a*-lipo and siRNA-*Hnf4α*-lipo decreased *Hnf4α* levels (Fig. 14A). Furthermore, the variants' downregulation over *Hnf4α* is more consistent between the two biological replicates when compared to *Notch2* (Fig. 14B). Variant 4 had the highest downregulation efficiency (median relative expression decrease to 0.69). In contrast, variant 6 had the lowest downregulation proficiency on *Hnf4α* (median relative expression increase to 1.33). Thus, after 12h, variant 6 demonstrated to be quite selective since it downregulated *Notch2* with a median fold decrease of 0.50 and upregulated *Hnf4α* with a fold increase of 0.33.

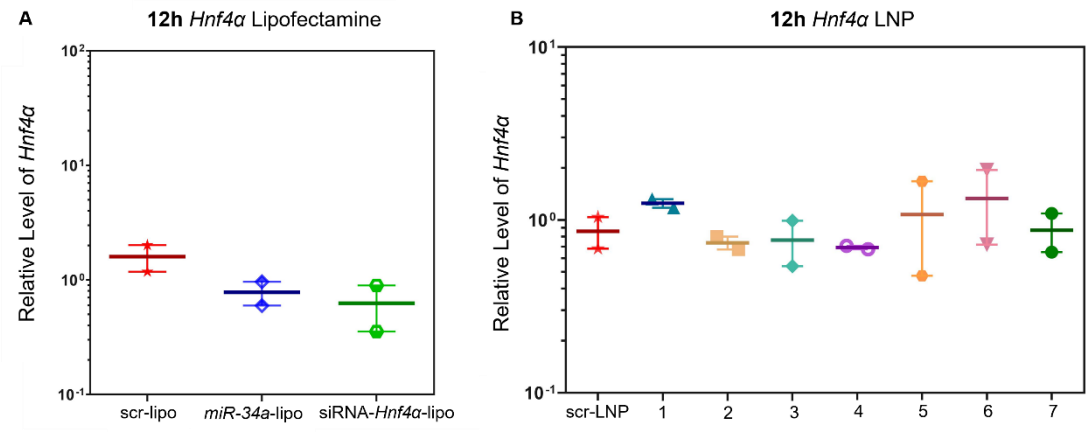

Figure 14 - RT-qPCR results of *Hnf4α* mRNA relative expression after 12h of transfection in isolated E13.5 hepatoblasts with two biological replicates. A) miRs transfected with lipofectamine: scrambled control (scr-lipo); *miR-34a* (*miR-34a*-lipo) and siRNA (siRNA-*Hnf4α*-lipo) transfected with RNAiMAX. B) Samples: scrambled control transfected with LNPs (scr-LNP); *miR-34a* 1, 2, 3, 4, 5, 6, 7 transfected with LNPs (*miR-34a*-LNP). Samples normalised to non-transfected cells set as 1.00. Statistical analysis was performed with the one-tailed Mann-Whitney statistical test.

Hepatoblasts can either differentiate into hepatocytes or cholangiocytes. *Sox9* is a cholangiocyte marker, whereas *Hnf4α* is a hepatocyte marker. Therefore, the downregulation of *Hnf4α* is expected to lead to a *Sox9* increase in expression levels. Furthermore, *Notch2* expression directly depends on *Sox9* expression [29]. Thus, the upregulation of *Notch2* likely results from increased *Sox9* expression levels. Due to the inter-correlation between *Sox9* and the two target genes, the expression of *Sox9*, 12h after *miR-34a* transfection, was also analysed. Transfection of *miR-34a-lipo* and siRNA-*Hnf4α*-lipo resulted in increased *Sox9* expression levels (Fig. 15A). In contrast, the *miR-34a*-LNP transfection had almost no effect on *Sox9* levels (Fig. 15B). This infers that 12h is insufficient time to see an indirect impact on *Sox9* upon *miR-34a*-LNPs transfection.

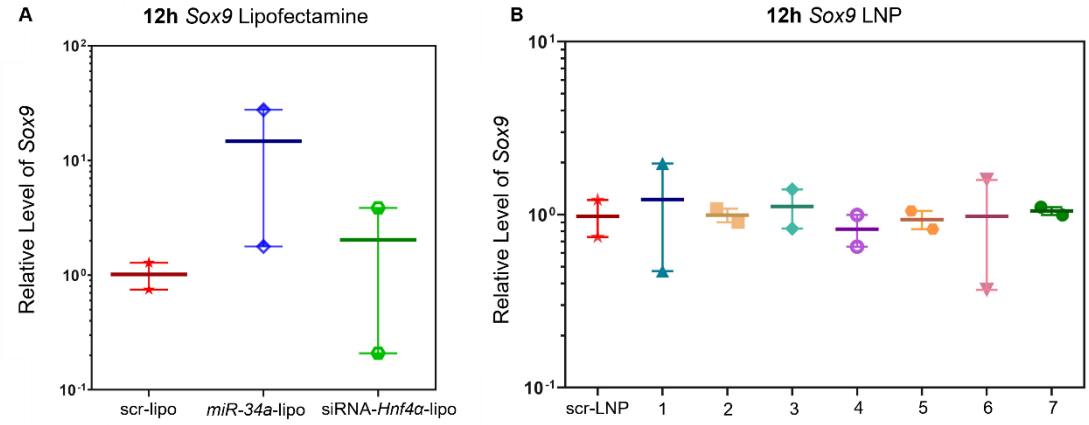

Figure 15 - RT-qPCR results of *Sox9* mRNA relative expression after 12h of transfection isolated E13.5 hepatoblasts with two biological replicates. A) miRs transfected with lipofectamine: scrambled control (scr-lipo); *miR-34a* (*miR-34a*-lipo) and siRNA (siRNA-*Hnf4α*-lipo) transfected

with RNAiMAX. B) Samples: scrambled control transfected with LNPs (scr-LNP); *miR-34a* 1, 2, 3, 4, 5, 6, 7 transfected with LNPs (*miR-34a*-LNP). Samples normalised to non-transfected cells were set as 1.00. Statistical analysis was performed with the one-tailed Mann-Whitney statistical test.

3. 24h long culture time leads to increased *miR-34a* activity

Since 12h of *miR-34a* activity was insufficient to acquire statistically significant and reproducible conclusions, the next step was assessing how the results would change with a longer transfection time. Accordingly, the following experiment was conducted with a 24h time-point in non-differentiating media with three biological replicates. Firstly, the transfection efficiency of the miRs-lipo was examined (Fig. 16A). The relative levels of *miR-34a* after scr-lipo transfection remained unchanged. While transfection with *miR-34a-lipo* considerably augmented levels of *miR-34a*, which was statistically significant, suggesting the presence of exogenous miRNA. Cells transfected with siRNA-*Hnf4α*-lipo had a lower variability between the three biological replicates, with a median *miR-34a* relative fold increase of 1.78. Similar to the 12-hour culture time, this slight increase can be explained by the fact that siRNA has been demonstrated to alter the endogenous levels of miRNA [89].

As for the *miR-34a*-LNPs (Fig. 16B), variant 6 showed the highest transfection efficiency with a median relative fold increment of 139.09. However, it also demonstrated the most variability among replicates. In contrast, variant 3 exhibited minor transfection efficiency with a median fold rise of 24.72. Interestingly, the transfection efficiency of variant 1 is lower than in the 12h experiment, but the result is statistically significant. This may indicate that the lack of chemical modification can make the molecule more prone to enzyme degradation, which decreases intracellular perseverance with time. In contrast, the level of *miR-34a* upon transfection with variant 5 is higher than in the 12h experiment. Variant 5 contains the 5'-PHOS and two PS bonds at each end of the molecule. Similarly to variant 4, PS bonds at the 5' and 3'-ends seem to efficiently protect the molecule and ensure its persistence after 24h of culture, which is represented by a statistically significant increase of *miR-34a* upon transfection with variant 4.

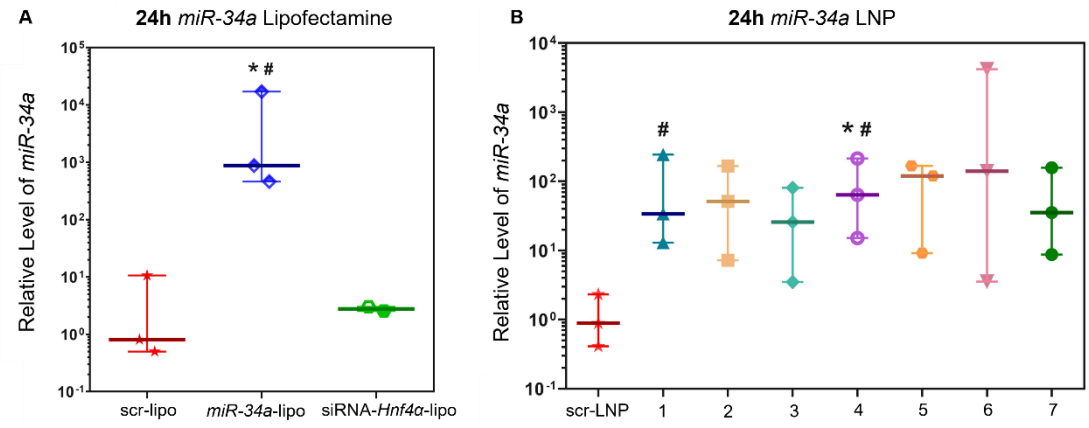

Figure 16 - RT-qPCR results of *miR-34a* relative expression after 24h transfection isolated E13.5 hepatoblasts with three biological replicates. A) miRs transfected with lipofectamine: scrambled control (scr-lipo); *miR-34a* (*miR-34a*-lipo) and siRNA (siRNA-*Hnf4α*-lipo) transfected with RNAiMAX. B) Samples: scrambled control transfected with LNPs (scr-LNP); *miR-34a* 1, 2, 3, 4, 5, 6, 7 transfected with LNPs (*miR-34a*-LNP). Samples normalised to non-transfected cells set as 1.00. Statistical analysis with Mann-Whitney test, statistically significant results ($p<0.0500$) marked as: (*) sample/NT control; (#) sample/scramble control.

The *Notch2* downregulation efficiency after 24h was also measured for the miRs-lipo (Fig. 17A) and *miR-34a*-LNPs (Fig. 17B). The relative expression of *Notch2* when the cells were transfected with the scr-lipo was 0.90. When cells were transfected with the *miR-34a*-lipo and siRNA-*Hnf4α*-lipo, the median levels declined to 0.59 and 0.75, respectively. Thus, after 24h, *miR-34a*-lipo had a considerable *Notch2* downregulation capability.

Looking at the downregulation efficiency among variants, it is feasible to detect some downregulation variability among replicates (Fig. 17B). Even though variant 1 intracellular persistence decreased after 24h, this variant had the highest efficiency in downregulating *Notch2* to a median expression level of 0.62. Likewise, variants 2 and 4 also led to a considerably *Notch2* downregulation. In contrast, the variant with the least downregulation efficiency was variant 6, which merely decreased *Notch2* relative expression to 0.95. This is a by-product of the five PS bonds that may have impaired the molecule's stability, decreasing its downregulation activity [90,91].

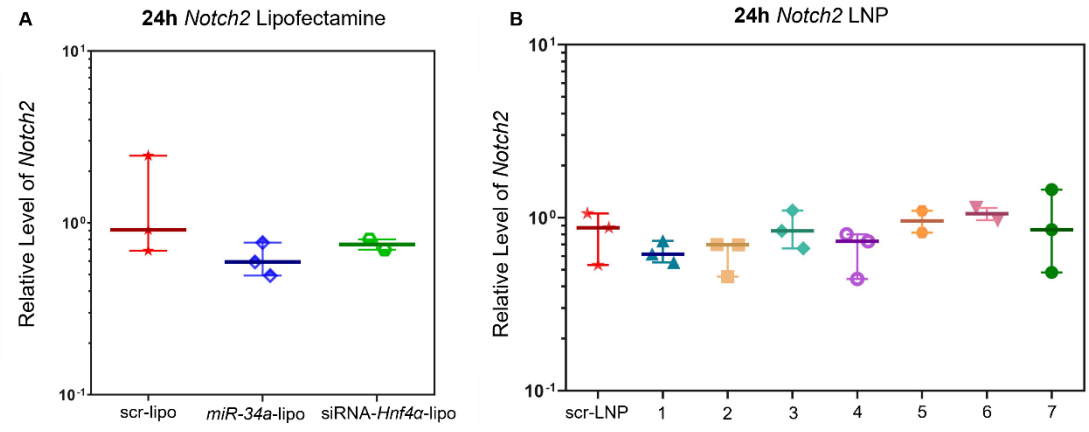

Figure 17 - RT-qPCR results of *Notch2* mRNA relative expression after 24h of transfection in isolated E13.5 hepatoblasts with three biological replicates. A) MiRs transfected with lipofectamine: scrambled control (scr-lipo); *miR-34a* (*miR-34a*-lipo) and siRNA (siRNA-*Hnf4α*-lipo) transfected with RNAiMAX. B) Samples: scrambled control transfected with LNPs (scr-LNP); *miR-34a* 1, 2, 3, 4, 5, 6, 7 transfected with LNPs (*miR-34a*-LNP). Samples normalised to non-transfected cells set as 1.00. Statistical analysis was performed with the one-tailed Mann-Whitney statistical test.

The levels of *Hnf4α* downregulation for the miRs-lipo and *miR-34a*-LNPs were then analysed. Similarly to *Notch2*, the scr-lipo led to a median fold decrease in *Hnf4α* relative level of 0.50. Similarly, both *miR-34a*-lipo and siRNA-*Hnf4α*-lipo decreased *Hnf4α* expression levels (Fig. 18A). Contractedly to *Notch2*, the downregulation efficiency among the variants was more reproducible between the three biological replicates (Fig. 18B). However, the downregulation between the variants was extremely close to that observed in the scr-LNP control (*Hnf4α* median expression level of 0.70).

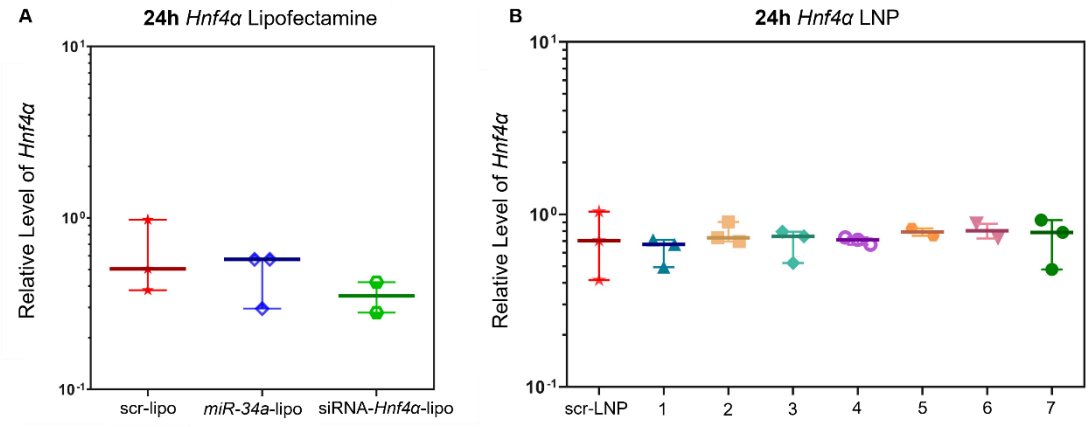

Figure 18 - RT-qPCR results of *Hnf4α* mRNA relative expression after 24h of transfection in isolated E13.5 hepatoblasts with three biological replicates. A) miRs transfected with lipofectamine: scrambled control (scr-lipo); *miR-34a* (*miR-34a*-lipo) and siRNA (siRNA-*Hnf4α*-lipo) transfected with RNAiMAX. B) Samples: scrambled control transfected with LNPs (scr-LNP); *miR-34a* 1, 2, 3, 4, 5, 6, 7 transfected with LNPs (*miR-34a*-LNP). Samples normalised to non-transfected cells set as 1.00. Statistical analysis was performed with the one-tailed Mann-Whitney statistical test.

To conclude the 24h time-point analyses, *Sox9* miRs downregulation was measured. Once again, there was downregulation of *Sox9* in the presence of the three miRs transfected with lipofectamine (Fig. 19A). Transfection with siRNA-*Hnf4α*-lipo led to the least variability between biological replicates. Among the replicates, one of the experiments gave a much lower expression of *Sox9* than the other two, which decreased reproducibility (Fig. 19B). This may be correlated to the high variability also seen for *Notch2* downregulation.

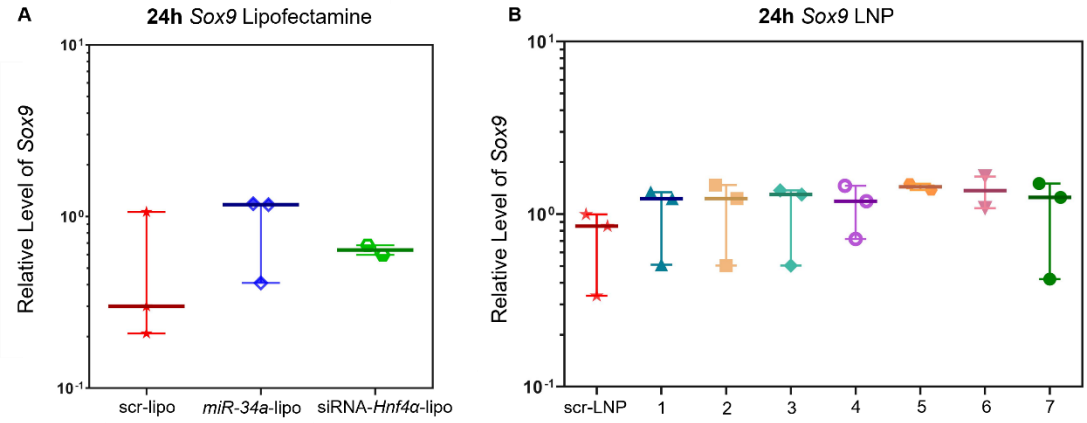

Figure 19 - RT-qPCR results of *Sox9* mRNA relative expression after 24h transfection in isolated E13.5 hepatoblasts with three biological replicates. A) MiRs transfected with lipofectamine: scrambled control (scr-lipo); *miR-34a* (*miR-34a-lipo*) and siRNA (siRNA-*Hnf4α*-lipo) transfected with RNAiMAX. B) Samples: scrambled control transfected with LNPs (scr-LNP); miR-34a 1, 2, 3, 4, 5, 6, 7 transfected with LNPs *(*miR-34a-*LNP)*. Samples normalised to non-transfected cells set as 1.00. Statistical analysis was performed with the one-tailed Mann-Whitney statistical test.

4. Improved *miR-34a* activity is reached after 48h

The next experiment was devised with an increased culture time of 48h. This was achieved to see if a longer *miR-34a* activity time would yield more defined results. Additionally, four biological replicates were performed in non-differentiating media under the same conditions to improve the reproducibility of the results.

The 48h transfection time-point resulted in a high *miR-34a* level in all three miRs transfected with lipofectamine (Fig. 20A). However, in scr-lipo, the *miR-34a* relative level had a fold increase of 1.15. This increment has been seen throughout the experiments and is extremely low compared to the effects of the *miR-34a-lipo* (median fold rise of 4673.89). Statistically significant results were achieved for *miR-34a* transfection when normalised with NT cells and cells transfected with scr-lipo. This validates H_1, which states that the treatment sample differs from the control one.

Figure 20B shows the *miR-34a*-LNP's transfection efficiency results with respective statistical analyses. Variants 1 (p=0.0143), 2 (p=0.0143), 4 (p=0.0143), 5 (p=0.0143), 6 (p=0.0286) and 7 (p=0.0143) led to a statistically significant increase in *miR-34a* levels compared to NT cells. Furthermore, normalised with the scr-LNP, variants 1 (p=0.0286) and 4 (p=0.0143) showed

significant higher levels of *miR-34a*. After 48h, transfection with variants 4, 1 and 5 led to an increased relative level of *miR-34a*. Namely, variant 4 led to a *miR-34a* median fold rise of 452.19.

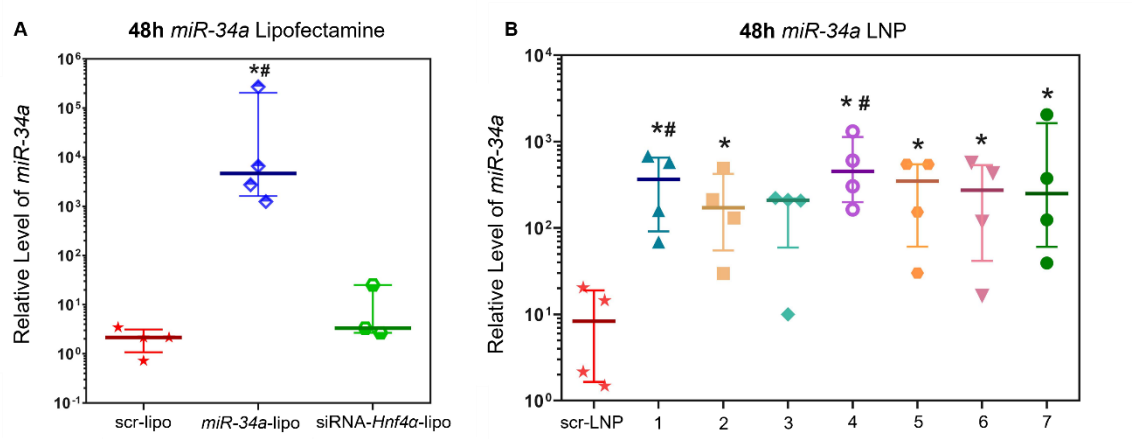

Figure 20 - RT-qPCR results of *miR-34a* relative expression after 48h transfection isolated E13.5 hepatoblasts with four biological replicates. A) MiRs transfected with lipofectamine: scrambled control (scr-lipo); *miR-34a* (*miR-34a*-lipo) and siRNA (siRNA-*Hnf4α*-lipo) transfected with RNAiMAX. B) Samples: scrambled control transfected with LNPs (scr-LNP); *miR-34a* 1, 2, 3, 4, 5, 6, 7 transfected with LNPs (*miR-34a*-LNP). Samples normalised to non-transfected cells set as 1.00. Statistical analysis with Mann-Whitney test, statistically significant results ($p<0.0500$) marked as: (*) sample/NT control; (#) sample/scramble control.

In contrast, variant 2 had the lowest persistence in the cell after 48h. This variant mimics the endogenous *miR-34a* with only a 5'-PHOS. Thus, this molecule may be more easily recognised by nucleases, and its loading to the Argonaute protein may be more efficient and, therefore, faster. This would lead to a quicker decay which would explain its lower levels after 48h. Similarly, variant 3 also had low *miR-34a* levels after 48h. This variant only differs from variant 2 by its PS bond at the 5'-end. Therefore, this chemical modification is insufficient to protect the molecule. Whereas variant 4, with one PS bond at each end, had a much higher intracellular persistence evidencing the importance of a PS bond at the 3'-end.

Following, *Notch2* downregulation after 48h was analysed. The scr-lipo control and siRNA-*Hnf4α*-lipo led to a slight downregulation which may have resulted from the mild increase in *miR-34a* expression levels (Fig. 21A). The transfection of the positive control *miR-34a-lipo* successfully downregulated *Notch2* to a median expression level of 0.27.

Looking at the results from the variants' downregulation efficiencies (Fig. 21B), it is feasible to see that all variants could substantially downregulate *Notch2* compared to the NT cells. However, variant 6 did not downregulate *Notch2* compared to the scr-LNP negative control. As expected, variant 4 had the highest downregulation efficiency over *Notch2* to a median expression level of 0.36. Variant 4 high efficiency can be correlated with its higher persistence in the cells after 48h. Thus, *miR-34a* persistence in the cell is directly related to its downregulation capability.

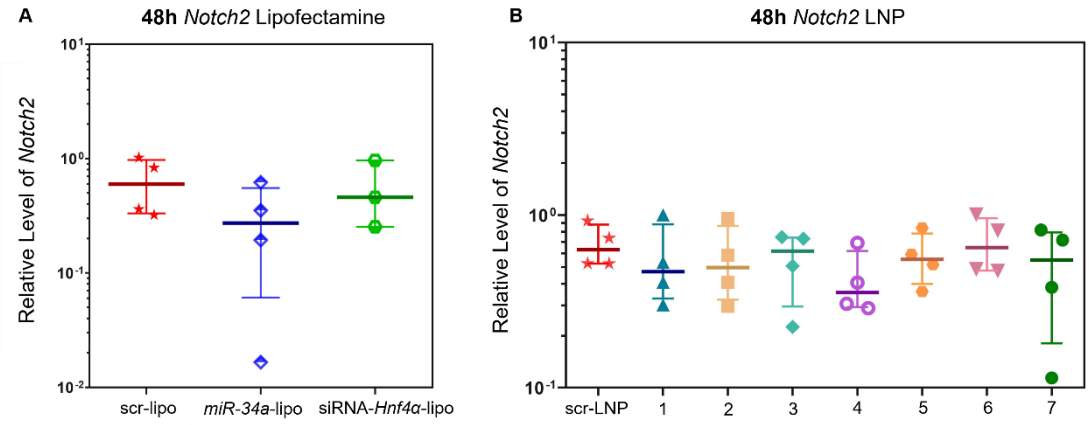

Figure 21 - RT-qPCR results of *Notch2* mRNA relative expression after 48h transfection isolated E13.5 hepatoblasts with four biological replicates. A) MiRs transfected with lipofectamine: scrambled control (scr-lipo); *miR-34a* (*miR-34a*-lipo) and siRNA (siRNA-*Hnf4α*-lipo) transfected with RNAiMAX. B) Samples: scrambled control transfected with LNPs (scr-LNP); *miR-34a* 1, 2, 3, 4, 5, 6, 7 transfected with LNPs (*miR-34a*-LNP). Samples normalised to non-transfected cells set as 1.00. Statistical analysis was performed with the one-tailed Mann-Whitney statistical test.

For *Hnf4α*, transfection with scr-lipo had almost zero effect on the levels of this gene (Fig. 22A). Both miRs-lipo downregulated *Hnf4α* to a median expression level equal to 0.34 and 0.33 for *miR-34a-lipo* and siRNA-*Hnf4α*-lipo, respectively. Furthermore, *miR-34a-lipo* downregulation over *Hnf4α* was statistically significant compared to the NT (p=0.0143) and scr-lipo control (p=0.0286). In contrast, siRNA-*Hnf4α*-lipo downregulation was only statistically significant compared to the NT cells (p=0.0286).

By analysing the results from the *miR-34a*-LNP's downregulation efficiency (Fig. 22B), it is possible to conclude that variant 2 was the most efficient in downregulating *Hnf4α* (median expression of 0.41), followed by variant 4 (median expression of 0.43). Although variant 2 intracellular levels were not optimal, it still efficiently downregulated *Hnf4α*. Thus, since variant 2 resembles the natural form of *miR-34a*, this may be an advantage because the cell machinery may recognise this molecule more efficiently, leading to a faster and more efficient downregulation capability, despite the more rapid decay. Nevertheless, molecules with slight modifications evidenced higher difficulty downregulating the target genes even though they had higher intracellular levels after 48h. For instance, variant 3 only differs from variant 2 by one 5'-end PS bond however it had a 0.19 relative expression increase of *Hnf4α*, whereas variant 2 had the highest downregulation capability. Statistical significance was achieved for variants 2 (p=0.0286) and 4 (p=0.0286). Hence, these variants led to a statistically significant decrease in *Hnf4α* expression compared to the non-transfected control.

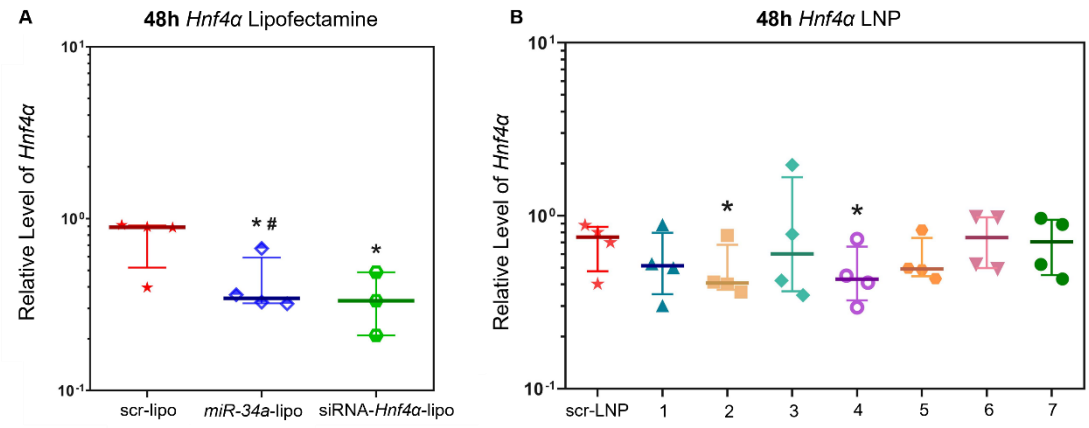

Figure 22 - RT-qPCR results of *Hnf4α* mRNA relative expression after 48h transfection isolated E13.5 hepatoblasts with four biological replicates. A) MiRs transfected with lipofectamine: scrambled control (scr-lipo); *miR-34a* (*miR-34a*-lipo) and siRNA (siRNA-*Hnf4α*-lipo) transfected with RNAiMAX. B) Samples: scrambled control transfected with LNPs (scr-LNP); *miR-34a* 1, 2, 3, 4, 5, 6, 7 transfected with LNPs (*miR-34a*-LNP). Samples normalised to non-transfected cells set as 1.00. Statistical analysis with Mann-Whitney test, statistically significant results ($p<0.0500$) marked as: (*) sample/NT control; (#) sample/scramble control.

Sox9 expression levels were also assessed after 48h. It is possible to see that *Sox9* levels increased more when cells were transfected with siRNA-*Hnf4α*-lipo than with *miR-34a*-lipo (Fig. 23A). This suggests that *Sox9* expression levels tend to be higher when *Hnf4α* is more downregulated when compared to *Notch2*. It is assumed that by downregulating *Hnf4α*, hepatoblast differentiation will shift from the default hepatocyte differentiation pathway to a cholangiocyte lineage. Furthermore, siRNA-*Hnf4α*-lipo elevated *Sox9* expression levels statistically differed from *Sox9* levels when cells were transfected with the negative scr-lipo control when applied to the Mann-Whitney statistical test ($p=0.0286$). Variant 4 transfection resulted in the smallest rise in *Sox9* levels (Fig. 23B) despite being the most efficient variant in downregulating both target genes.

To conclude, after 48h, due to the lack of reproducibility, no solid conclusion can be made regarding variants' indirect impact on *Sox9* expression levels. The indirect effect from each *miR-34a* variant over *Sox9* varied greatly between replicates. Nonetheless, a pattern can be envisaged when comparing *miR-34a* downregulation of its two target genes to *Sox9* relative expression. Overall, the downregulation of the two target genes, *Notch2* and *Hnf4α,* leads to a rise in *Sox9* expression, as was visualised for all three-time points. However, when this downregulation is more accentuated, *Sox9* expression levels increase less. This was verified for variant 4, which significantly downregulated both target genes while its transfection had little interference over *Sox9* expression levels. However, when cells were transfected with variants 1 or 7, there was not a significant decrease in target gene expression, but the expression levels of *Sox9* increased substantially. Therefore, there is no direct effect between *Notch2* and *Hnf4α* downregulation and an increase in *Sox9* expression levels.

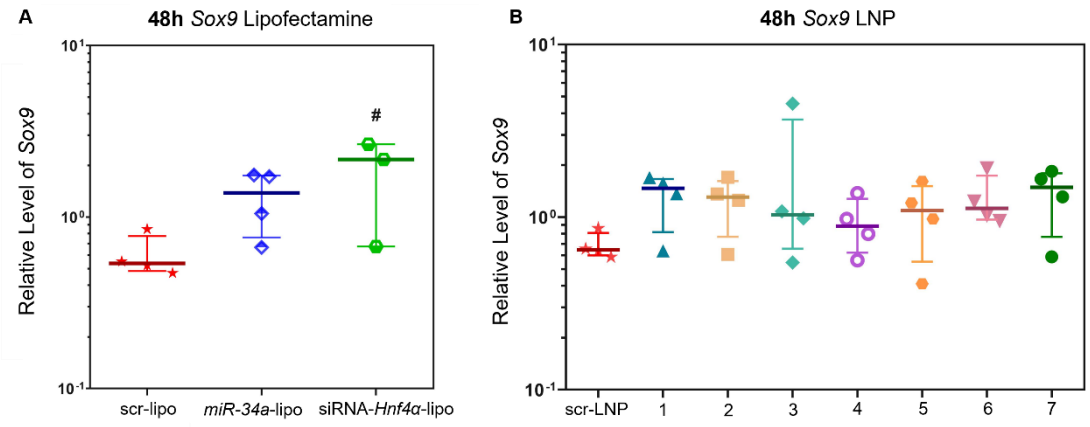

Figure 173 - RT-qPCR results of *Sox9* mRNA relative expression after 48h transfection isolated E13.5 hepatoblasts with four biological replicates. A) MiRs transfected with lipofectamine: scrambled control (scr-lipo); *miR-34a* (*miR-34a*-lipo) and siRNA (siRNA-*Hnf4α*-lipo) transfected with RNAiMAX. B) Samples: scrambled control transfected with LNPs (scr-LNP); *miR-34a* 1, 2, 3, 4, 5, 6, 7 transfected with LNPs (*miR-34a*-LNP). Samples normalised to non-transfected cells set as 1.00. Statistical analysis with Mann-Whitney test, statistically significant results ($p<0.0500$) marked as: (*) sample/NT control; (#) sample/scramble control.

5. After 72h, hepatoblasts began differentiation

During hepatic embryogenesis, it is known that hepatoblasts differentiate into hepatocytes as the default mechanism [13]. Hepatocyte differentiation increases the expression of hepatocyte marker *Hnf4α* [64]. However, hepatoblasts can also differentiate into cholangiocytes leading to an increase in *Sox9*, the marker for cholangiocyte differentiation [22]. Hence, another question that needs to be answered is whether transfection with *miR-34a*-LNP can modulate hepatoblast differentiation into hepatocyte or cholangiocyte lineage.

To answer this question, hepatoblasts were transfected with *miR-34a* seven variants and cultured in differentiating media for 72h. Furthermore, cells were cultured with a bottom layer of fibronectin and an upper layer of Matrigel. Matrigel can mimic cell-extracellular matrix interactions and maintain the self-renewal capability of pluripotent cells [92]. Thus, hepatoblasts were cultured with a double-layered matrix since they require physical support for the correct morphological change during differentiation [93]. The culture medium was supplemented with hepatocyte growth factor (HGF) and epidermal growth (EGF) essential for hepatoblast expansion, maturation, and maintenance of self-renew capability [94,95]. For this experiment, only one biological replicate was performed. Thus, no statistical analysis was performed.

The miRs transfected with lipofectamine followed the same pattern as the previous results (Fig. 24A). The scr-lipo and siRNA-*Hnf4α*-lipo slightly increased *miR-34a* expression, while *miR-34a-lipo* resulted in a substantial median fold increase on *miR-34a* levels of 15904.7. This shows that even with a longer transfection time, *miR-34a* seems to be stable in the intracellular space. As for

the variants, overall, variant 4 had the highest transfection efficiency with a median fold increase in *miR-34a* levels of 2335.0 when compared to the non-transfected sample (Fig. 24B).

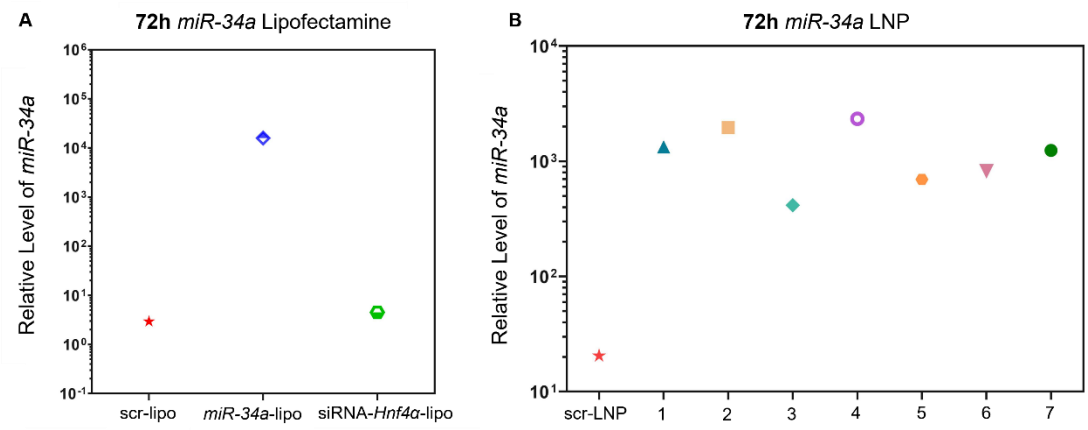

Figure 184 - RT-qPCR results of *miR-34a* relative expression after 72h transfection isolated E13.5 hepatoblasts with one biological replicate. A) MiRs transfected with lipofectamine: scrambled control (scr-lipo); *miR-34a* (*miR-34a*-lipo) and siRNA (siRNA-*Hnf4α*-lipo) transfected with RNAiMAX. B) Samples: scrambled control transfected with LNPs (scr-LNP); *miR-34a* 1, 2, 3, 4, 5, 6, 7 transfected with LNPs (*miR-34a*-LNP). Samples normalised to non-transfected cells set as 1.00.

When looking at the downregulation efficiency over *Notch2*, it seems that after 72h, *miR-34a-lipo* is no longer active (Fig. 25A). In fact, *Notch2* was slightly upregulated when compared to the negative controls. Transfection with siRNA-*Hnf4α*-lipo led to a high downregulation of *Notch2*, which strengthens the premise that the siRNA might have an off-target effect on the *Notch2* gene. Additionally, it may be concluded that all *miR-34a*-LNPs retained their activity after 72h (Fig. 25B). Transfection with variants 2 and 4 had a median decrease in *Notch2* expression levels to 0.26 and 0.28, respectively. Only variants 7 and 3 had almost no effect on *Notch2* relative expression. To conclude, even after inducing differentiation, most of the variants seem to downregulate *Notch2*.

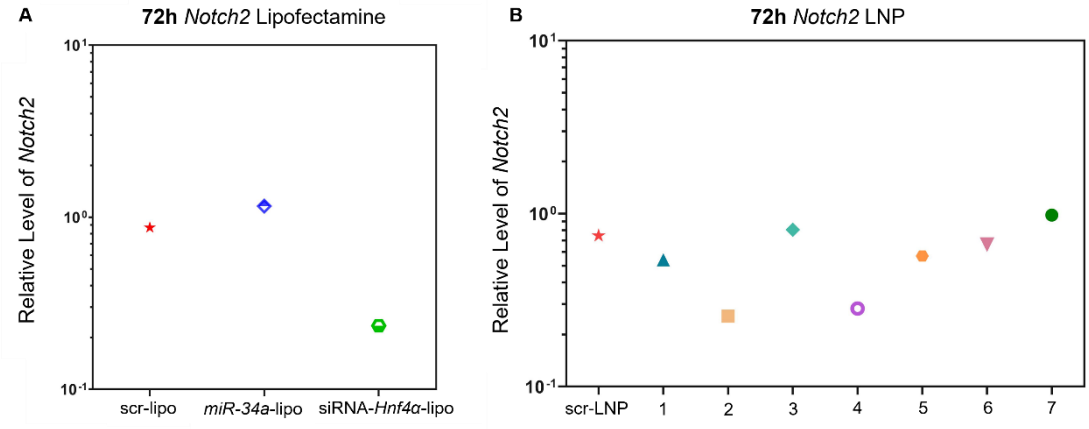

Figure 195 - RT-qPCR results of Notch2 mRNA relative expression after 72h transfection isolated

E13.5 hepatoblasts with one biological replicate. A) MiRs transfected with lipofectamine: scrambled control (scr-lipo); miR-34a (miR-34a-lipo) and siRNA (siRNA-Hnf4α-lipo) transfected with RNAiMAX. B) Samples: scrambled control transfected with LNPs (scr-LNP); miR-34a 1, 2, 3, 4, 5, 6, 7 transfected with LNPs *(*miR-34a-*LNP)*. Samples normalised to non-transfected cells set as 1.00. Samples normalised to non-transfected cells set as 1.00.

Results for *Hnf4α* downregulation efficiency after 72h are presented in Figures 26A and 26B. Similarly to *Notch2*, *miR-34a-lipo* was probably no longer active after 72h. Regarding the variants' downregulation over *Hnf4α*, the results differed from the pattern observed until this point. All variants downregulated *Hnf4α* more when compared to the NT control. However, different results were achieved when their downregulation efficiency was compared to transfection with the scr-LNP. Only variants 1 and 3 downregulated *Hnf4α* more than the scrambled control. Variant 4, which previously had the highest downregulation efficiency on *Hnf4α*, after 72, had an almost null effect over *Hnf4α* expression (median expression level decrease only to 0.93).

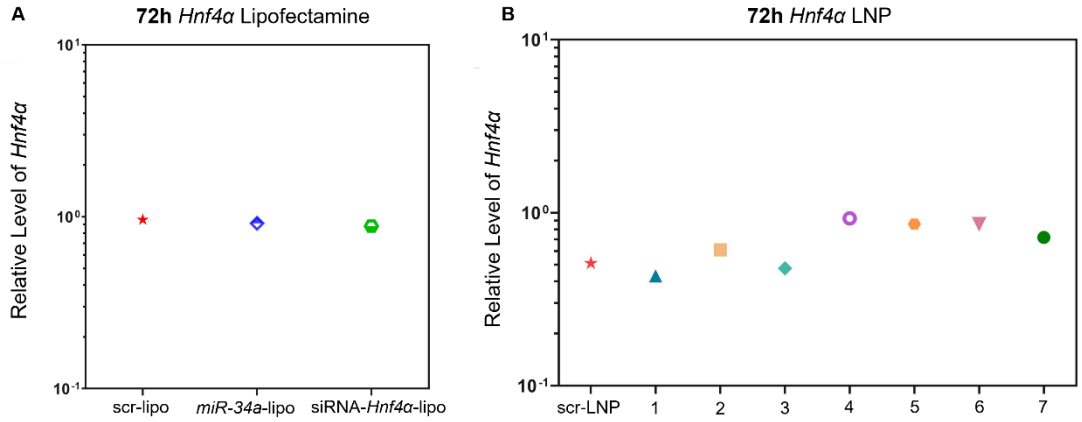

Figure 206 - RT-qPCR results of *Hnf4α* mRNA relative expression after 72h transfection isolated E13.5 hepatoblasts with one biological replicate. A) MiRs transfected with lipofectamine: scrambled control (scr-lipo); *miR-34a* (*miR-34a*-lipo) and siRNA (siRNA-*Hnf4α*-lipo) transfected with RNAiMAX. B) Samples: scrambled control transfected with LNPs (scr-LNP); *miR-34a* 1, 2, 3, 4, 5, 6, 7 transfected with LNPs (*miR-34a*-LNP). Samples normalised to non-transfected cells set as 1.00.

Sox9 downregulation after 72h was also assessed. Scr-lipo and *miR-34a-lipo* did not significantly change *Sox9* expression (Fig. 27A). Only transfection with siRNA-*Hnf4α*-lipo resulted in an increase in the relative level of *Sox9* to 1.31. Regarding the results of *Sox9* expression after *miR-34a*-LNP transfection, these are highly similar to the ones obtained for *Notch2* (Fig. 27B). Thus, after 72h of transfection, under differentiating conditions, the levels of *Sox9* tend to decrease for most variants, as occurred in *Notch2*. This may prove that *Notch2* and *Sox9* expressions directly depend on one another.

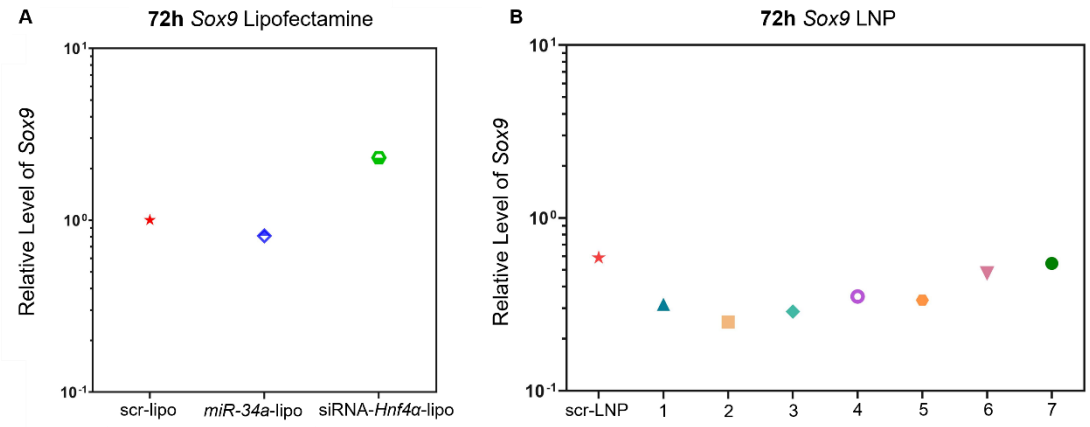

Figure 217 - RT-qPCR results of *Sox9* mRNA relative expression after 72h transfection isolated E13.5 hepatoblasts with one biological replicate. A) MiRs transfected with lipofectamine: scrambled control (scr-lipo); *miR-34a* (*miR-34a*-lipo) and siRNA (siRNA-*Hnf4α*-lipo) transfected with RNAiMAX. B) Samples: scrambled control transfected with LNPs (scr-LNP); *miR-34a* 1, 2, 3, 4, 5, 6, 7 transfected with LNPs (*miR-34a*-LNP). Samples normalised to non-transfected cells set as 1.00.

Variant 7 had similar results to the scr-LNP control in the three studied genes. Thus, it is possible to conclude that after 72h, variant 7 downregulation efficiency decreases even further. Overall, after 72h, variants 4 and 2 were the ones that led to noticeable changes in the expression of the three genes.

In this experiment, differentiation may be observed by *Notch2* increased downregulation, which was less noticeable for variants 3 and 7. This observation may be coupled with a decrease in *Hnf4α* downregulation, especially for variant 4. These two remarks are characteristic of hepatic specification. Additionally, *Sox9* expression levels were similar to *Notch2,* which confirms the inter-dependence between these two genes.

The beginning of differentiation of the hepatoblasts after 72h can be observed in Figure 28. This image was taken to non-transfected cells after 72h in differentiating media. It is possible to visualise that hepatoblasts started differentiating into hepatocytes by their change in morphology and an initial formation of bile canaliculi. During liver development, hepatoblasts differentiate into hepatocytes [93]. The hepatocytes start sharing their apical surface with differentiation, forming an anisotropic 3D network known as bile canaliculi [93]. This result confirms the start of hepatocyte differentiation and also supports the observations made with RT-qPCR.

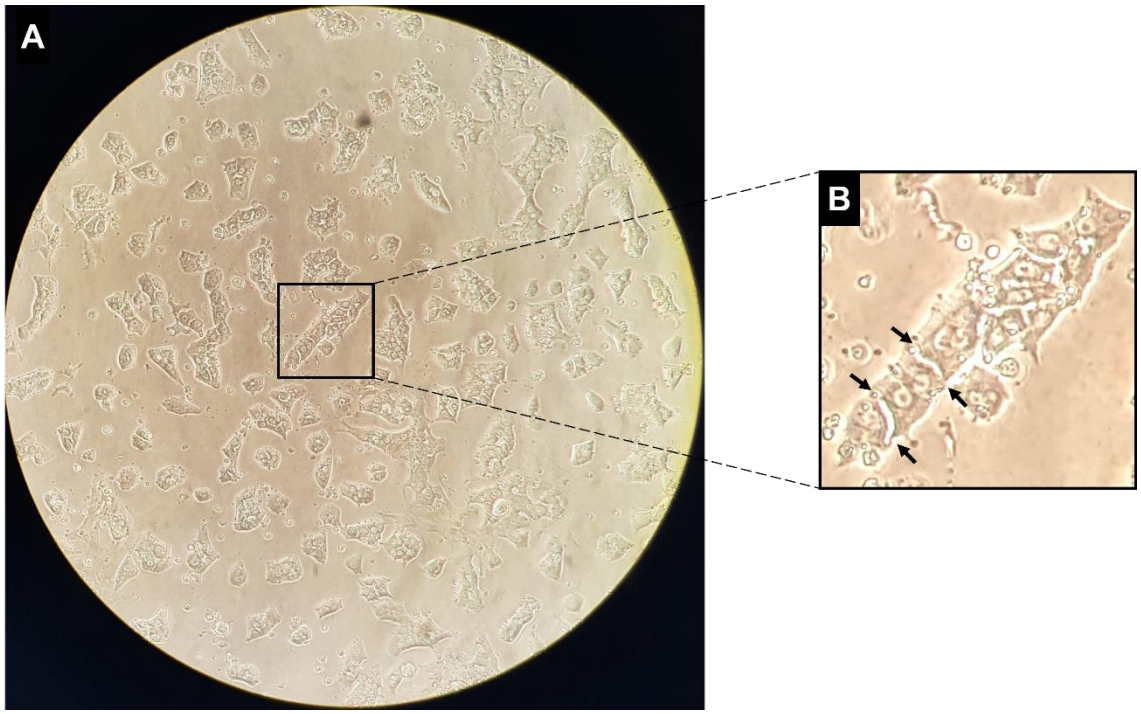

Figure 228 - A) Microscopic image of was taken in an optical microscope at 40x magnification of non-transfected cells after 72h of cell culture. B) Amplification of a section of the microscopic image zoomed in on the formation of the bile canaliculi marked by the arrows.

6. *miRNA-34*-LNP downregulates *Hnf4α* via translation repression and mRNA degradation

With the RT-qPCR analysis, it was possible to see that the *miR-34a*-LNPs could downregulate *Notch2* and *Hnf4α*. However, miRNAs can downregulate target genes by translation repression or mRNA degradation [54,55]. Therefore, the levels of mRNA target genes are expected to decrease when mRNA is degraded, as seen by the qPCR results. Nevertheless, if the translation is inhibited, protein levels will also decline. To determine which mechanism *miR-34a* uses to downregulate *Hnf4α*, a Western blot was performed to assess Hnf4α protein levels after 48h of transfection. For normalisation purposes, B-actin was used as a loading control.

Firstly, it was possible to detect the 42kDa band for B-actin and the 52kDa band for Hnf4α (Fig .29A) [96]. The control's results confirmed the qPCR data (Fig. 29B). Generally, scr-lipo slightly decreased the Hnf4α level to 0.60. In contrast, *miR-34a*-lipo and siRNA-*Hnf4α*-lipo decreased Hnf4α protein levels to 0.13 and 0.32, respectively. Variants 6 and 7 had almost no effect on Hnf4α protein levels. In contrast, variants 3 and 4 reduced protein levels to 0.38 and 0.44, respectively (Fig. 29C). Their protein downregulation is comparable to the one achieved on cells transfected with siRNA-*Hnf4α*-lipo specific for *Hnf4α*. The median values for variants 3 and 4 downregulation on mRNA *Hnf4α* were 0.60 and 0.43, respectively. Thus, Hnf4α downregulation with variant 3 is more noticeable at the protein levels than at the mRNA level. Accordingly, it can be assumed that variant 3 downregulates *Hnf4α* more via translation inhibition. The values for variant 4 were similar for mRNA and protein downregulation efficiency.

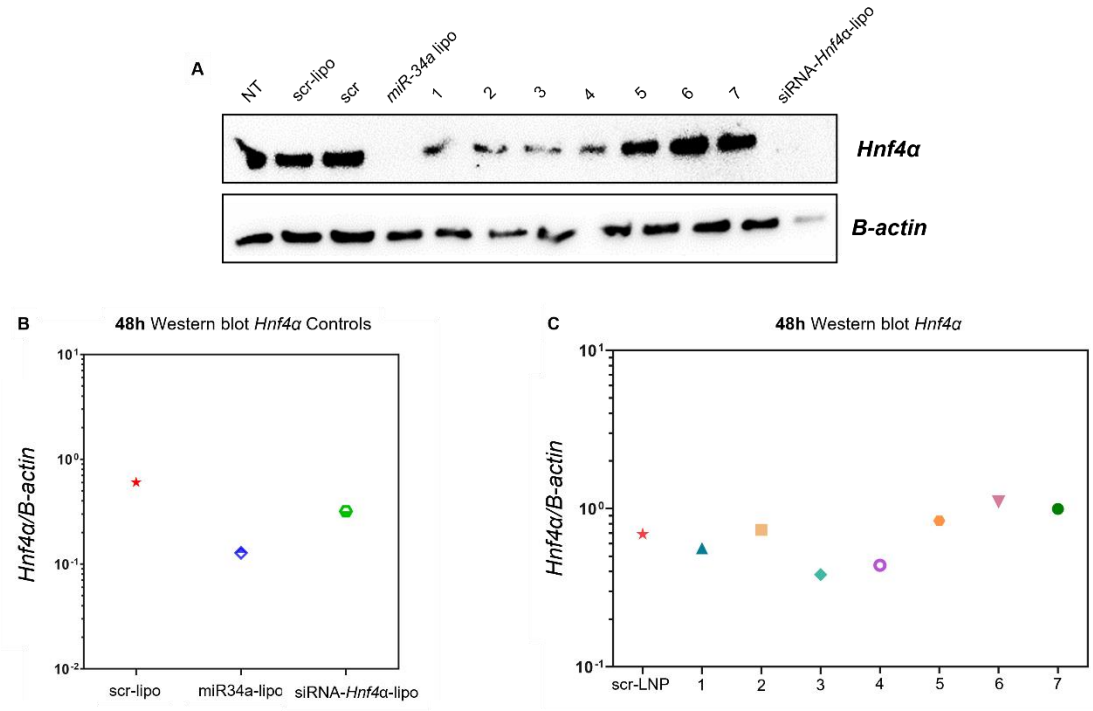

Figure 239 - Western blot analysis of Hnf4α protein after 48h of transfection in E13.5 isolated hepatoblasts. A) Results processed in ImageLabTM version 6.0.1 software. B) MiRs transfected with lipofectamine: scrambled control (scr-lipo); *miR-34a* (*miR-34a*-lipo) and siRNA (siRNA-*Hnf4α*-lipo) transfected with RNAiMAX. C) Samples: scrambled control transfected with LNPs (scr-LNP); *miR-34a* 1, 2, 3, 4, 5, 6, 7 transfected with LNPs (*miR-34a*-LNP).

Genes with a *miR-34a* 3'UTR binding site tend to be downregulated via translation inhibition [57]. However, *miR-34a* can modulate the expression of several genes by mRNA degradation and translation repression since, for *miR-34a*, the two downregulation mechanisms are co-regulated [57]. More specifically, *miR-34a* can decrease *Hnf4α* mRNA levels in the liver by 40% while decreasing protein expression to 75% [97]. In the results, the preference for translation repression of *miR-34a* over *Hnf4α* is not as noticeable for most variants except for variant 3. However, probably both downregulation mechanisms can be detected for most variants used in this study. Thus, it is assumed that *miR-34a* can downregulate hepatic *Hnf4α* levels via translation repression and mRNA degradation.

7. Intracellular localisation of *Hnf4α* after transfection

The observation made in RT-qPCR showed that *miR-34a* transfected hepatoblasts can initiate differentiation when cultured for 72h in differentiating media. Furthermore, the data suggest a shift in the *miR-34a* capability of downregulating *Hnf4α*. We assume that as differentiation proceeds, *Hnf4α* expression starts to increase gradually. Thus, replicates of the same cells used for the RT-qPCR experiment were utilised for Hnf4α and DAPI staining. This was performed to determine Hnf4α changes at the protein level within the cell as differentiation starts. This analysis was performed in cells transfected with all the variants. The results after cell transfection with variants 2, 3, 4, and 7 are showed in Figure 30. After 72h in differentiating media, the co-localization of

Hnf4α and DAPI is evident which indicates that most of the expressed Hnf4α was in the nucleus. During normal hepatic differentiation from the endoderm, Hnf4α is mainly localised in the nucleus [98]. Hnf4α retention in the cytoplasm is primarily associated with hepatic diseases such as NAFLD [99].

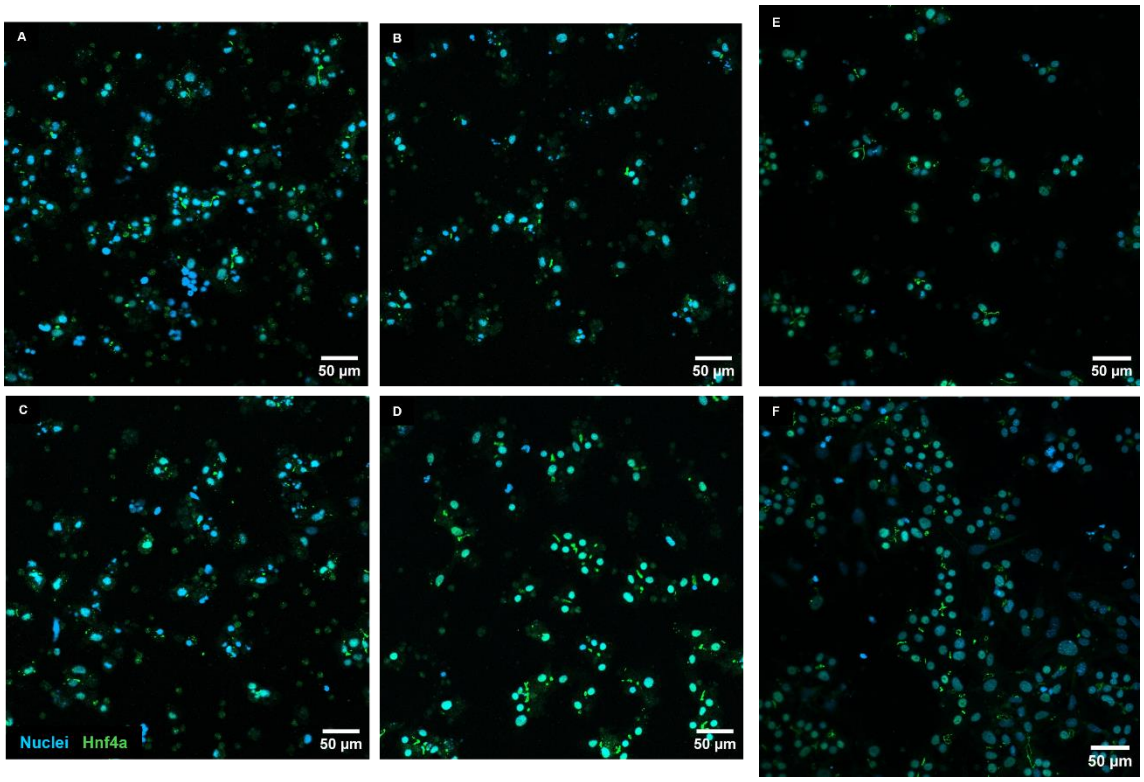

Figure 3024 - E13.5 hepatoblasts stained for Hnf4α and DAPI (Alexa fluor anti-rabbit 488 1:500 and DAPI 1:1000), imaged with a Zeiss LSM 900 Airyscan confocal microscope. Cells transfected with A) *miR-34a* 2 LNP. B) *miR-34a* 3 LNP C) *miR-34a* 4 LNP D) *miR-34a* 7 LNPs E) siRNA-*Hnf4α*-lipo. F) Non-transfected cells.

Discussion

This work aimed to evaluate the effectiveness and stability of *miR-34a* delivered to E13.5 mouse hepatoblasts using lipid nanoparticles as a transfection agent. Additionally, *miR-34a* was also transfected with lipofectamine to compare how the used LNPs enhanced this delivery.

Successful *miR-34a* delivery with LNPs in the intracellular space depends on the internalisation mechanism and efficacy of the endosomal escape strategy. The delivery of *miR-34a* with the formulated LNPs in primary hepatic cells has not been done before. However, the utilised LNPs are mainly constituted by the ionisable lipid C12-200, which have been evidenced to promote cell uptake via macropinocytosis [100–102]. Furthermore, C12-200 ionisable lipids can avoid early lysosomal degradation, fusing directly with the endosomes upon internalisation. Once inside the endosomes, the lipids from the LNPs form an ion pair with the lipids of the endosomal membrane. This interaction will modify the endosomal membrane into a non-bilipid structure (Fig. 9). This leads to membrane rupture and miRNA release to the cytoplasm [75]. It is believed that the formulated LNPs can be internalised and escape the endosomes in this manner. The efficiency and stability of *miR-34a* delivered by lipid nanoparticles were assessed primarily with RT-qPCR.

To validate the qPCR results, negative controls were prepared. Throughout the experiments, transfection of the scr-lipo and scr-LNP often led to a low increment in *miR-34a* levels. However, the increased level of *miR-34a* may not have been a direct cause of scrambled *miR-34a* transfection. Hepatoblasts are sensible progenitor cells that adjust rapidly in 2D culture since, after isolation, they can endure functional and phenotypic changes [103]. Thus, some gene expression variations upon seeding were expected. As *miR-34a* is involved in various physiological functions, it is possible that as the progenitor cells change upon seeding, the expression of this miRNA may also naturally fluctuate.

The transfection efficiency was also validated with *miR-34a*-lipo and siRNA-*Hnf4α*-lipo. Transfection of siRNA-*Hnf4α*-lipo with RNAiMAX also often led to a slight increase in *miR-34a* expression levels. However, this increase may also not be utterly correlated with siRNA transfection. In the 3'UTR region of *Hnf4α*, there are three binding sites for *miR-34a* [104]. Thus, *miR-34a* will bind to the *Hnf4α* mRNA and prevent its translation. However, transfection with siRNA decreases the *Hnf4α* mRNA expression, probably leading to less mRNA available for *miR-34a* binding. Thus, presumably, more *miR-34a* is left unbound, which could explain the increased relative level of *miR-34a* in these cells. Furthermore, the presence of siRNA has been demonstrated to modulate the expression of some miRNAs [89]. Generally, siRNA transfection decreases miRNA expression due to competition with the Argonaute protein. However, in some cases, siRNA transfection can also increase miRNA endogenous levels. Thus, the presence of siRNA affects specific miRNAs differently depending on Argonaute availability and the affinity between siRNA and miRNA for the protein. In addition, some miRNAs can remain active by binding to other proteins to compensate for the inaccessible Argonaute protein [89].

The validation of the used controls in RT-qPCR was crucial to analyse how efficient was the proposed transfection method. However, since the LNP transfection mechanism was new to the literature, it was also essential to determine the adequate transfection time to attain high intracellular *miR-34a* levels.

After 12h of *miR-34a* activity, no downregulation was observed among the *miR-34a*-LNP variants on *Notch2* and *Hnf4α.* Furthermore, neither target gene was significantly downregulated even after transfecting the cells with *miR-34a*-lipo. Therefore, 12h may be insufficient time for *miR-34a* to downregulate these two target genes effectively. After increasing, the *miR-34a* transfection time to 24h, *miR-34a*-LNP transfection and downregulation efficacy did improve. Even so, the LNP's transfection efficiency results exhibit a lack of reproducibility between biological replicates. Consequently, it is possible to conclude that 24h may be still not enough time to achieve a stable transfection rate, intracellular persistence and successful activity. Maximum *miR-34a*-LNP transfection yield in this study was accomplished at the 48h time-point, which resulted in the highest *miR-34a* levels. Therefore, an increased time point with at least four biological replicates is sufficient to achieve statistical significance for most variants.

As for the 72h differentiation study, hepatic specification was detected. However, in these conditions only *Notch2* was observed to be downregulated, while no downregulation in *Hnf4α* was observed. This phenomenon was noticeable for most variants. It is predicted that as differentiation proceeds, the expression of *Hnf4α* will continue to increase. This strengthens the fact that after 48-72h of differentiation induction, hepatic genes start to be expressed. The levels of *Hnf4α* can increase almost 10-fold as differentiation proceeds [105]. Thus, after 72h, the levels of *Hnf4α* expression may surpass *miR-34a* downregulation capability since the degree of transcribed *Hnf4α* mRNA probably exceed the intracellular levels of *miR-34a*. This may have been the leading cause of *Hnf4α* increased expression levels.

Throughout the analysis of *miR-34a* downregulation over its target genes, it was possible to conclude that different chemical modifications led to distinct levels of downregulation. Therefore, besides establishing that 48h was the optimal time for *miR-34a*-LNP transfection, it was feasible to determine the most suitable chemical modifications for target gene regulation. To attain this, each variant's downregulation efficiency was individually assessed.

Variant 1 is composed only of the naked *miR-34a* sequence. As the transfection time increased, variant 1 intracellular persistence declined. Even so, after 12h, this variant had noticeable downregulation efficiency, suggesting that variant 1 can overcome degradation to a certain degree despite not having any chemical modification. One hypothesis to justify this short-term resistance is that the cell may recognise this variant more rapidly after transfection due to the lack of extra chemical modifications. This contradicts most miRNAs since the 5'-end phosphorylation is usually the determinant factor for miRNA activation [106,107]. After miRNA is synthesised and phosphorylated, it is loaded into Argonaute and processed into its fully matured form. Only then it becomes active. However, *miR-34a* is an exception to this rule. *miR-34a* activation seems to be dependent on a cellular stress factor [106]. After *miR-34a* synthesis, this molecule can be

sequestered in a miRNA intracellular pool [106]. Once the cell receives a stress signal, *miR-34a* is activated by a 5'-end phosphorylation. Only after this procedure *is miR-34a* loaded into the Argonaute protein to become fully matured [106]. Another hypothesis for variant 1's successful intracellular survival is that when dephosphorylated *miR-34a* is transfected to the cells, it still needs to be phosphorylated to be loaded into the Argonaute protein. As such, its complete maturation is hampered. Upon synthesis, if miRNA is not loaded in the Argonaute, it cannot undergo enzymatic activities related to decay, such as adding or removing nucleotides known as tailing and trimming, respectively [108]. Furthermore, once matured, miRNAs can have a half-life of up to 24h. Thus, from the time-point at which variant 1 is phosphorylated and becomes active, it can still survive for 24h [108]. All these factors may contribute to the resistance of this naked *miR-34a* variant.

In contrast, variant 2 achieved a better downregulation and transfection efficiency throughout the experiments. This variant represents the most natural form of *miR-34a* since it comprises its nucleotide sequence with the activation factor 5'-PHOS [106,107]. Therefore, it may be easily recognised by the cell machinery leading to an efficient loading into the Argonaute protein. However, the lack of chemical alterations makes it more susceptible to nucleases, which may limit its downregulation effectiveness. This would explain the quicker decay detected after 48h of transfection.

Compared to variant 2, variant 3 demonstrated a slightly lower transfection and downregulation efficiency over time. For example, after 12h, variant 3 had the lowest transfection efficiency among all the variants. Surprisingly, this molecule has a 5'-PHOS and a PS bond at the 5'-end. Thus, it is highly similar to variant 4, which, after 12h, had the second-highest downregulation efficiency, so it would be expected that these two variants have similar results. It is, thus, possible to conclude that a single PS bond at the 5'-end seems insufficient to protect the molecule against nuclease degradation.

Throughout the experiments, variant 4 had the best downregulation efficiency and transfection rate. It is feasible to infer that, among all variants, variant 4 had the highest and most stable transfection efficiency. This variant has a phosphate group at the 5'-end and one PS bond at the 5' and 3'-ends. The insertion of PS bonds substitutes the non-bridging phosphate oxygen in the phosphate backbone with sulphur, increasing internucleotide linkage resistance to nucleases [109]. Consequently, variant 4 is protected from exonuclease attacks at both ends, which leads to increased intracellular survival. This maintains high *miR-34a* levels, yielding high downregulation efficiency over both target genes.

Comparably to variant 4, variant 5 is phosphorylated at the 5'-end and contains two PS bonds at each end of the molecule. Overall, this variant presented moderate downregulation and transfection efficiency. PS bonds at the 5' and 3'-ends seem to efficiently protect the molecule and ensure its intracellular persistence over time. However, one more PS bond at each end decreased this variant's downregulation efficiency. Therefore, a single PS bond and each end is probably the optimal for transfection and downregulation effectiveness.

Variant 6 presented relatively low efficiency and high variability over time compared to the other variants. For example, after 12h, variant 6 was the most efficient in downregulating *Notch2*. This differs from the 24h time-point from which variant 6 had the least downregulation efficiency over this gene. This variant comprises a total of 5 bonds at its ends. Even though PS bonds can protect the molecule against enzyme degradation, PS substitutions can also decrease the thermal stability of the miRNA [90,91]. For each PS modification, the melting temperature is expected to fall from 0.5 to 0.7˚C [90,91]. Thus, five PS bonds may have impaired the molecule's stability, decreasing its downregulation activity. Moreover, this variant presented a high variability in terms of efficiency depending on the time point and target gene downregulation. For instance, it simultaneously had the highest downregulation efficiency over *Notch2* after 12h and the lowest downregulation efficiency over *Hnf4α*. Thus, after 12h of transfection, this variant also exhibited a high selectivity among the target genes.

Variant 7 also presented average downregulation efficiency, despite having a 5'-end vinyl phosphonate group. The 5'-end vinyl phosphonate group substitutes the 5'-phosphate since the unsaturated C-C bond restricts the group's torsion angle to 180º. This restriction mimics the optimal positioning of the natural existing phosphate group. Subsequently, this modification is expected to increase the affinity between the *miR-34a* and Argonaute protein by adapting the enzyme's binding site [110]. Furthermore, the 5'-end vinyl phosphonate can increase resistance to phosphatases surpassing the 5'-phosphate predispositions to dephosphorylation [111]. However, this study did not verify the expected effectiveness of this chemical modification.

Despite different variants exhibiting distinct efficiencies, after 48h, the studied *miR-34a* variants also presented downregulation selectivity between *Notch2* and *Hnf4α*. Figure 31 comprises the downregulation selectivity between *Notch2* and *Hnf4α* for each variant. Looking at this plot, it is feasible to observe that variants represented in orange tend to downregulate *Notch2* and *Hnf4α* equally. It is also discernible that variant 4 had the highest downregulation efficiency over *Notch2* and *Hnf4α*. Moreover, this downregulation was analogous between the two target genes. Contrarily, variant 6 had the lowest downregulation efficiency for both genes. Variants 3 and 7 are highlighted in green since they selectively downregulate one gene more than the other. Variant 3 tends to downregulate *Hnf4α* more efficiently than *Notch2*. In contrast, variant 7 preferentially downregulates *Notch2* more than *Hnf4α*.

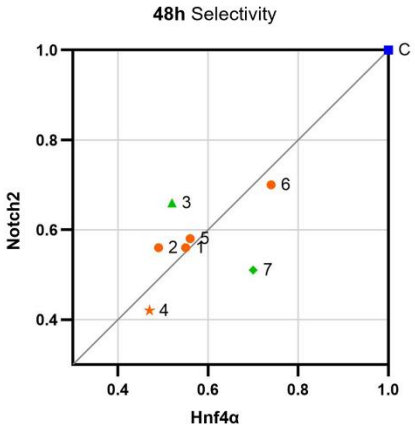

Figure 31 - Downregulation selectivity between *Notch2* and *Hnf4α*. A) MiRs transfected with lipofectamine: *miR-34a* (*miR-34a*-lipo) and siRNA (siRNA-*Hnf4α*-lipo) transfected with RNAiMAX in orange and non-transfected control (C) in blue. B) Samples: scrambled control transfected with LNPs (scr-LNP); *miR-34a* 1, 2, 3, 4, 5, 6,7 transfected with LNPs (*miR-34a*-LNP). Variants with similar downregulation between genes in orange. Variant 3 downregulates more *Hnf4α* (green triangle). Variant 7 downregulates more *Notch2* (green diamond). Non-transfected control in blue square.

It is common for miRNAs to have differential downregulation efficiency between distinct target genes. Their activity depends, among several factors, on seed pairing effectiveness [50]. It is crucial to have an accessible seed region for the correct binding between the miRNA and mRNA molecule. Furthermore, the lower the free energy of Gibbs of miRNA-mRNA duplex, the more stable this association, leading to more efficient interaction. The abundance of target sites from miRNA on the mRNA molecule can also improve downregulation [50].

However, miRNA selectivity knowledge is quite restricted. Thus, it is challenging to clarify why variant 7 preferentially downregulates *Notch2* while variant 3 favourably downregulates *Hnf4α*. Variant 3 has a 5'-PHOS with one PS at the 5'-end, differing from variant 7, which comprises a 5'-end vinyl phosphonate group with 2 PS bonds on both sides. As such, this selectivity could be explained either by the 5'-end or the backbone modification. The vinyl phosphonate group has two main functions that theoretically lead to higher activity. It can protect a miRNA against phosphatases, a common problem in miRNAs that have the 5'-PHOS as an activation factor. Furthermore, once the Argonaute protein detects the 5'-end vinyl phosphate modification, it can adjust its essential residues in the binding pocket to better interact with the miRNA. This enhances the interaction and leads to an improved silencing effect [112]. Still, improved downregulation was not observed in the attained results. Structurally, the vinyl phosphonate group is similar to the phosphate group. Thus, these molecules should be comparable in terms of volume and bulkiness, meaning that they should be equally accessible for mRNA target site binding [113]. The only factor that may change the overall structure of these two variants is the different number of PS bonds. A phosphorothioate bond tends to increase the distance between two adjacent nucleotides [114]. Thus, variant 7 may be more elongated than variant 3 which could interfere with target site

binding. However, variant 5 also has 4 PS bonds and did not exhibit downregulation selectivity. Therefore, neither the 5'-end nor the backbone modification clearly explains the observed selectivity. As such, more experiments would have to be conducted to explain miRNA selectivity over target genes confidently.

With the attained results, it is possible to conclude that the *miR-34a* variants distinctively regulated the expression of the two target genes. Some of the variants even displayed selectivity between *Notch2* and *Hnf4α*. Furthermore, after 48h of *miR-34a* transfection, the isolated hepatoblasts initiated hepatic specification. Subsequently, despite *miR-34a* not directly regulating *Sox9* expression, a pattern for *Sox9* expression levels after *miR-34a* transfection was delineated. By downregulating both target genes, there is a tendency for the expression of *Sox9* to increase. However, when this downregulation is greatly accentuated, as for variant 4, *Sox9* levels do not increase as much. If only *Hnf4α* ought to be downregulated, *Sox9* levels would most likely increase. However, *Notch2* has two binding sites, within its transcription start site, for *Sox9* [29]. When *Sox9* is overexpressed in murine livers, the expression of *Notch2* increases in a dependent manner through direct transcriptional activation [29]. Consequently, *Notch2* downregulation decreases *Sox9* expression, which minimises the increase that results from *Hnf4α* downregulation. Still, since variant 3 tends to downregulate more *Hnf4α* than *Notch2*, it would be expected for *Sox9* expression to increase after variant 3 transfection significantly. Likewise, by transfecting hepatoblasts with variant 7, which downregulates *Notch2* more than *Hnf4α*, the levels of *Sox9* were expected to decrease. These two characteristics were not evident in the obtained results. Subsequently, there is no linear relationship between *Hnf4α*/*Notch2* downregulation and *Sox9* levels. More experiments would have to be performed to confidently conclude from the obtained data.

Conclusion

A new life begins when two cells fuse to form a zygote [115]. This new unique cell can originate a complex organism through coordinated cell interactions, proliferation, and differentiation. In a matter of days, this cell forms a cellular mass known as the blastocyst. It is at this stage that the first differentiation event takes place. The further specification of these cells depends on the proper control of the gene expression. A complex network of signalling pathways, together with regulatory molecules, such as miRNAs, regulate the expression of these genes. When this regulatory system is disturbed, severe genetic disorders can arise, leading to embryo mortality or post-natal developmental illnesses [115].

The liver is a dynamic organ essential in various biological functions such as macronutrient metabolism, blood supply, immune responses, and digestion of xenobiotic compounds [2]. Subsequently, the liver function is tightly regulated by signalling pathways. However, severe developmental defects occur when these regulatory mechanisms fail, and genes are inaccurately expressed. For instance, deregulation of *Notch2* can lead to Alagille syndrome [28] and abnormal bile duct morphogenesis [23]. Furthermore, mutations in *Hnf4α* lead to malformations of the hepatic parenchyma [64]. *miR-34a* regulates the expression of these two genes and, thus, plays a crucial part during early development [63, 17].

As such, this work aimed to determine the influence that *miR-34a* regulation has over *Notch2* and *Hnf4α* during liver embryogenesis. By deciphering this, *miR-34a* could be used as a tool to modify and correct abnormal target gene expression, commonly found in embryonic defects and during pathogenesis. Accordingly, *miR-34a* was delivered to liver progenitor cells and its activity was assessed. However, nucleic acid delivery still faces limiting challenges. Subsequently, an innovative strategy using LNPs composed mainly of an ionisable lipid was exploited to deliver *miR-34a* into the isolated hepatoblasts. The delivered *miR-34a* contain several chemical modifications to surpass nuclease degradation. The subsequent analysis was performed to assess which modification would improve intracellular survival the most and lead to a more effective downregulation of the two target genes.

One of this work's milestones was optimising E13.5 hepatoblast isolation from the CD1 pregnant mice. Per experiment, around 24-26 embryonic livers were collected, which resulted in an average of 3.50×10^6 to 5.50×10^6 cells. This was achieved by firstly perfusing, digesting and lysing red blood cells from the collected livers. Afterwards, hepatoblasts with highly expressed DLK1 were isolated using magnetic beads that bind to DLK1-positive cells. Through trial and error, hepatoblasts were seeded in 96 well plates with an optimised cell density of 35 000 cells/well. The cells were cultured for 12, 24, and 48h in non-differentiating media and 72h in differentiating media.

After cell culture, miRNA and total mRNA were isolated from the hepatoblasts. The attained concentration of RNA depended on the sample and culture time. Overall, longer-term cell culture led to higher levels of isolated RNA. Furthermore, non-transfected cells had higher RNA

concentrations, while cells transfected with lipofectamine usually led to lower amounts of RNA. Thus, these cells proliferated less than cells transfected with the LNPs. This suggests that lipofectamine has a more detrimental effect on cell survival during culture and might be more cytotoxic than the used LNPs. However, more studies should be performed to support this hypothesis.

The cell culture in non-differentiating media from 12 to 48h allowed the study of *miR-34a*-LNP transfection and downregulation efficiency over time. After 12h of *miR-34a* transfection there was no significant downregulation from the *miR-34a*-LNPs nor from the lipofectamine transfected molecules. As such, 12h may be insufficient time for effective *miR-34a* activity. Upon 24h of transfection, there was an increase in *miR-34a* activity for all the tested variants. Despite the increased miRNA activity, there was a high discrepancy in downregulation efficiency among the three biological replicates in all variants. Therefore, the next step was to increase the transfection time to 48h with four biological replicates. With this culture time, it was still possible to detect high levels of *miR-34a*-LNP in the transfected samples, which indicates a good transfection efficiency and stability of the molecules after 48h. Thus, the study resulted in up to 0.64- and 0.59-fold downregulation of *Notch2* and *Hnf4α*, respectively, making 48h optimal culture time among the studied time points.

The 72h long transfection of *miR-34a*-LNP on the isolated progenitor cells enabled the assessment of the influence of *miR-34a* downregulation over the two target genes and hepatic specification. Even after *miR-34a* transfection, the expression of *Notch2* and *Hnf4α* was characteristic of hepatoblast differentiation. Downregulation of *Notch2* was more pronounced than for *Hnf4α*. *Hnf4α* was still downregulated after *miR-34a* transfection however, its decrease in expression started to lessen. Thus, it is suggested that as differentiation starts, the expression levels of *Hnf4α* may surpass *miR-34a* downregulation proficiency. It is expected that by increasing transfection time even further, the expression of *Hnf4α* would gradually increase.

Throughout the experiments, *miR-34a* variants with different chemical modifications led to distinct downregulation efficiencies. The naked variant 1 surprisingly managed to resist intracellular degradation when the transfection time was shorter. Suggesting that variant 1 may be less recognised by the cellular machinery, which delays its loading in the Argonaute protein and its decay. Even so, this molecule's intracellular resistance decreases with increased culture time. Variant 2 represents the wild-type form of *miR-34a* and, thus, had average downregulation efficiency and intracellular resistance over the different time points compared to other variants. Thus, the 5'-PHOS leads to an increased and more stable miRNA regulatory effectiveness. Compared to variant 2, variant 3 demonstrated lower transfection and downregulation effectiveness. In contrast, variant 4 presented the best downregulation efficiency with high intracellular resistance compared to other *miR-34a* variants. This variant has a phosphate group at the 5'-end and one PS bond at the 5' and 3'-ends. Thus, it harbours PS bonds at each end, shielding the molecule against enzyme degradation. However, increasing the number of PS bonds does not always lead to improved activity, as was seen with variants 5 and 6. Variant 5

has phosphorylation at the 5'-end and two PS bonds at each end. However, this variant also presented moderate downregulation compared to other *miR-34a* variants. This was further evidenced by variant 6, which has 5 PS bonds at its ends. Despite PS bonds improving intracellular resistance, too many of these chemical modifications can decrease the thermal stability of the molecule, as one PS modification increases the melting temperature from 0.5 to 0.7˚C. Therefore, one PS at each end is probably the optimal number for maximum *miR-34a* activity in hepatoblasts. Another striking result was attained for variant 7. This molecule has a 5'-end vinyl phosphonate group, which has been shown to protect nucleic acids exceptionally efficiently and improve Argonaute binding [110, 127]. This would increase stability in the cell and downregulation efficiency, respectively. However, this was not observed in the obtained results. This variant had overall average transfection and regulation effectiveness compared to other variants.

The experimented *miR-34a* variants presented downregulation selectivity between *Notch2* and *Hnf4α*. Variant 7 exhibited increased downregulation efficiency over *Notch2*. In contrast, variant 3 preferentially downregulated *Hnf4α*. The two variants diverged from each other by the 5'-end modification and the number of PS bonds. When considering the phosphorothioate substitution, variant 3 and variant 4 had similar amounts of PS modifications. In parallel, variant 7 and variant 5 had an equal number of PS linkages. Thus, the selectivity does not seem to be linked to this type of modification. Otherwise, a similar preferential silencing would be observed in other variants. Regarding the 5'-end modification, adding the vinyl phosphonate group did not improve downregulation efficiency nor change the overall structure of the molecule. As such, it is impossible to confidently explain the observed variants' target selectivity with the attained data. Thus, more experiments would have to be conducted to determine if these chemical modifications could have changed other physicochemical parameters that might have influenced target gene selectivity.

Regarding the variants' downregulation over *Sox9*, no direct correlation was attained between *Notch2* and *Hnf4α* downregulation and *Sox9* expression levels. Nevertheless, a pattern was identified. Overall, the downregulation of the two target genes led to increased expression levels of *Sox9*. However, when the downregulation of *Notch2* and *Hnf4α* was too strong, the expression levels of *Sox9* stopped increasing as much. *Notch2* possibly caused this since its and *Sox9*'s expression levels dependently correlate. As the levels of *Notch2* reduce, the levels of *Sox9* also decline despite de decrease in *Hnf4α* expression.

Future Work

The findings of this study provided important insights into nucleic acid delivery and miRNA therapies. However, the attained results must be polished and moulded into more solid conclusions. To achieve this, additional experiments ought to be designed.

For example, the time point analysis, in non-differentiating media, was conducted up until 48h. It would be valuable to determine the culture time from which transfection of *miR-34a*-LNP would cease. It would also be essential to have more biological replicates to achieve statistical confidence in all variants. Furthermore, differentiation was only assessed for 72h and with only one biological replicate. As such, more biological replicates of 72h and experiments with longer culture times should be done to have more conclusive results regarding the hepatic specification. Ideally, modulating hepatic specification to cholangiocyte or hepatocyte fate would be possible. This could be used, for instance, in ALGS since by promoting cholangiocyte specification, the bile duct paucity could be reverted into a healthy and fully functional biliary system. Furthermore, from the obtained results, it is still not viable to take conclusions from *miR-34a's* indirect effect on *Sox9* expression. As such, more biological replicates would contribute to more confident conclusions. It would also be essential to test alternative *miR-34a* chemical modifications. Ideally similar to the ones in variant 4 as it gave the best results. Doing this would enable us to determine even more efficient modifications. This would also give more information regarding target selectivity observed for some variants. Thus, it would be possible to downregulate *Notch2* or *Hnf4α* with increased precision and efficiency.

Moreover, it would also be noteworthy to determine more precisely how the naked variant 1 can persist in the intracellular space after 48h. For example, this variant could be tagged with a signalling molecule, such as in a molecular beacon, so it would be possible to track it over time within the cell. Molecular beacons are oligonucleotide hybridisation probes with a quencher and a fluorophore at each end of the molecule. When there is no complementary molecule, the molecular beacon is closed, and no fluorescence is emitted. However, when there is a complementary sequence, it can bind to it, distancing the quencher from the fluorophore, and thus fluorescence is detected. By transforming variant 1 into a molecular beacon, it would be possible to localise this variant in the cell and detect its hybridisation with a target gene. Thus, it would be possible to confirm that variant 1 activity on target genes.

The ultimate experiment would be to repeat this analysis *in vivo*. This would be achievable since LNPs have reduced toxicity in mice [116]. However, several parameters would need to be optimised. For instance, the *miR-34a*-LNPs delivery method targets progenitor cells. This could be done while embryos are still in the uterus. Efforts to *in vivo* inject the mouse embryos have already been made in ERA Lab at Karolinska Institutet. The NEPTUNE technique (neural plate targeting by in-utero nano injection) was developed to deliver molecules, such as lentiviruses, in early stages mouse embryos [117]. This technique enables the delivery of lentivirus in E7.5 mouse embryos' brains. In future, this technique could be utilised to deliver the miRNAs into the E13.5 mouse embryos and target the gene expression.

References

1. Tam, P. P. L. & Behringer, R. R. Mouse gastrulation: The formation of a mammalian body plan. *Mech Dev* **68**, 3–25 (1997).

2. Trefts, E., Gannon, M. & Wasserman, D. H. The liver. **27**, (2018).

3. Yang, L. *et al.* The contributions of mesoderm-derived cells in liver development. *Semin Cell Dev Biol* **92**, 63–76 (2019).

4. Ober, E. A. & Lemaigre, F. P. Development of the liver: Insights into organ and tissue morphogenesis. *J Hepatol* **68**, 1049–1062 (2018).

5. Tremblay, K. D. & Zaret, K. S. Distinct populations of endoderm cells converge to generate the embryonic liver bud and ventral foregut tissues. *Dev Biol* **280**, 87–99 (2005).

6. Gordillo, M., Evans, T. & Gouon-Evans, V. Orchestrating liver development. *Development (Cambridge)* **142**, 2094–2108 (2015).

7. Bort, R., Signore, M., Tremblay, K., Martinez Barbera, J. P. & Zaret, K. S. Hex homeobox gene controls the transition of the endoderm to a pseudostratified, cell emergent epithelium for liver bud development. *Dev Biol* **290**, 44–56 (2006).

8. Zorn, A. M. Liver development. in (2008). doi:10.3824/stembook.1.25.1.

9. Serls, A. E., Doherty, S., Parvatiyar, P., Wells, J. M. & Deutsch, G. H. Different thresholds of fibroblast growth factors pattern the ventral foregut into liver and lung. *Development* **132**, 35–47 (2005).

10. Rossi, J. M., Dunn, N. R., Hogan, B. L. & Zaret, K. S. Distinct mesodermal signals, including BMPs from the septum transversum mesenchyme, are required in combination for hepatogenesis from the endoderm. *Genes Dev* **15**, 1998–2009 (2001).

11. Tachmatzidi, E. C., Galanopoulou, O. & Talianidis, I. Transcription control of liver development. *Cells* **10**, 1–20 (2021).

12. Si-Tayeb, K., Lemaigre, F. P. & Duncan, S. A. Organogenesis and Development of the Liver. *Dev Cell* **18**, 175–189 (2010).

13. Yang, L. *et al.* A single-cell transcriptomic analysis reveals precise pathways and regulatory mechanisms underlying hepatoblast differentiation. *Hepatology* **66**, 1387–1401 (2017).

14. Lotto, J. *et al.* Single-Cell Transcriptomics Reveals Early Emergence of Liver Parenchymal and Non-parenchymal Cell Lineages. *Cell* **183**, 702-716.e14 (2020).

15. Slim, C. L. *et al.* Par1b Induces Asymmetric Inheritance of Plasma Membrane Domains via LGN-Dependent Mitotic Spindle Orientation in Proliferating Hepatocytes. *PLoS Biol* **11**, (2013).

16. Gissen, P. & Arias, I. M. Structural and functional hepatocyte polarity and liver disease. *J Hepatol* **63**, 1023–1037 (2015).

17. Babeu, J. P. & Boudreau, F. Hepatocyte nuclear factor 4-alpha involvement in liver and intestinal inflammatory networks. *World J Gastroenterol* **20**, 22–30 (2014).

18. Watt, A. J., Garrison, W. D. & Duncan, S. A. HNF4: A central regulator of hepatocyte differentiation and function. *Hepatology* vol. 37 1249–1253 Preprint at https://doi.org/10.1053/jhep.2003.50273 (2003).

19. Parviz, F. *et al.* Hepatocyte nuclear factor 4α controls the development of a hepatic epithelium and liver morphogenesis. *Nat Genet* **34**, 292–296 (2003).

20. Boyer, J. L. Bile formation and secretion. *Compr Physiol* **3**, 1035–1078 (2013).

21. Banales, J. M. *et al.* Cholangiocyte pathobiology. *Nat Rev Gastroenterol Hepatol* **16**, 269–281 (2019).

22. Antoniou, A. *et al.* Intrahepatic Bile Ducts Develop According to a New Mode of Tubulogenesis Regulated by the Transcription Factor SOX9. *Gastroenterology* **136**, 2325–2333 (2009).

23. Geisler, F. *et al.* Liver-specific inactivation of Notch2, but not Notch1, compromises intrahepatic bile duct development in mice. *Hepatology* **48**, 607–616 (2008).

24. Antoniou, A. *et al.* Intrahepatic Bile Ducts Develop According to a New Mode of Tubulogenesis Regulated by the Transcription Factor SOX9. *Gastroenterology* **136**, 2325–2333 (2009).

25. Ming, Z., Vining, B., Bagheri-Fam, S. & Harley, V. SOX9 in organogenesis: shared and unique transcriptional functions. *Cellular and Molecular Life Sciences* **79**, (2022).

26. Adams, J. M. & Jafar-Nejad, H. The roles of notch signaling in liver development and disease. *Biomolecules* **9**, 1–20 (2019).

27. Kopan, R., Chen, S. & Liu, Z. Alagille, Notch, and robustness: why duplicating systems does not ensure redundancy. *Pediatr Nephrol* **29**, 651–657 (2014).

28. Gilbert, M. A. *et al.* Alagille syndrome mutation update: Comprehensive overview of JAG1 and NOTCH2 mutation frequencies and insight into missense variant classification. *Hum Mutat* **40**, 2197–2220 (2019).

29. Adams, J. M. *et al.* Sox9 Is a Modifier of the Liver Disease Severity in a Mouse Model of Alagille Syndrome. *Hepatology* **71**, 1331–1349 (2020).

30. Saliminejad, K., Khorram Khorshid, H. R., Soleymani Fard, S. & Ghaffari, S. H. An overview of microRNAs: Biology, functions, therapeutics, and analysis methods. *J Cell Physiol* **234**, 5451–5465 (2019).

31. Dexheimer, P. J. & Cochella, L. MicroRNAs: From Mechanism to Organism. *Front Cell Dev Biol* **8**, 1–18 (2020).

32. Kozomara, A. & Griffiths-Jones, S. MiRBase: Annotating high confidence microRNAs using deep sequencing data. *Nucleic Acids Res* **42**, 68–73 (2014).

33. Ozsolak, F. *et al.* Chromatin structure analyses identify miRNA promoters. *Genes Dev* **22**, 3172–3183 (2008).

34. Stucki, M. *et al.* Structure of Human DROSHA. *Cell* **164**, 81–90 (2016).

35. Annese, T., Tamma, R., de Giorgis, M. & Ribatti, D. microRNAs Biogenesis, Functions and Role in Tumor Angiogenesis. *Front Oncol* **10**, 1–21 (2020).

36. Nguyen, T. A., Park, J., Dang, T. L., Choi, Y.-G. & Kim, V. N. Microprocessor depends on hemin to recognize the apical loop of primary microRNA. *Nucleic Acids Res* **46**, 5726–5736 (2018).

37. Auyeung, V. C., Ulitsky, I., McGeary, S. E. & Bartel, D. P. Beyond secondary structure: primary-sequence determinants license pri-miRNA hairpins for processing. *Cell* **152**, 844—858 (2013).

38. Partin, A. C. *et al.* Heme enables proper positioning of Drosha and DGCR8 on primary microRNAs. *Nat Commun* **8**, 1737 (2017).

39. Kwon, S. C. *et al.* Molecular Basis for the Single-Nucleotide Precision of Primary microRNA Processing. *Mol Cell* **73**, 505-518.e5 (2019).

40. Lund, E., Güttinger, S., Calado, A., Dahlberg, J. E. & Kutay, U. Nuclear Export of MicroRNA Precursors. *Science (1979)* **303**, 95–98 (2004).

41. Miller, S., Jones, L. E., Giovannitti, K., Piper, D. & Serra, M. J. Thermodynamic analysis of 5' and 3' single- and 3' double-nucleotide overhangs neighboring wobble terminal base pairs. *Nucleic Acids Res* **36**, 5652–5659 (2008).

42. Schirle, N. T., Sheu-Gruttadauria, J. & MacRae, I. J. Structural basis for microRNA targeting. *Science (1979)* **346**, 608–613 (2014).

43. Wee, L. M., Flores-Jasso, C. F., Salomon, W. E. & Zamore, P. D. Argonaute divides its RNA guide into domains with distinct functions and RNA-binding properties. *Cell* **151**, 1055–1067 (2012).

44. Broughton, J. P., Lovci, M. T., Huang, J. L., Yeo, G. W. & Pasquinelli, A. E. Pairing beyond the Seed Supports MicroRNA Targeting Specificity. *Mol Cell* **64**, 320–333 (2016).

45. Grosswendt, S. *et al.* Unambiguous identification of miRNA:target site interactions by different types of ligation reactions. *Mol Cell* **54**, 1042–1054 (2014).

46. Sheu-Gruttadauria, J., Xiao, Y., Gebert, L. F. & MacRae, I. J. Beyond the seed: structural basis for supplementary micro RNA targeting by human Argonaute2 . *EMBO J* **38**, 1–14 (2019).

47. Grimson, A. *et al.* MicroRNA targeting specificity in mammals: determinants beyond seed pairing. *Mol Cell* **27**, 91–105 (2007).

48. Belter, A. *et al.* Mature miRNAs form secondary structure, which suggests their function beyond RISC. *PLoS One* **9**, 1–23 (2014).

49. Plata, C. A., Marni, S., Suweis, S., Bellini, T. & Paraboschi, E. M. Needles in Haystacks: Understanding the Success of Selective Pairing of Nucleic Acids. *Int J Mol Sci* **23**, (2022).

50. Riolo, G., Cantara, S., Marzocchi, C. & Ricci, C. miRNA targets: From prediction tools to experimental validation. *Methods and Protocols* vol. 4 1–20 Preprint at https://doi.org/10.3390/mps4010001 (2021).

51. Medley, J. C., Panzade, G. & Zinovyeva, A. Y. microRNA strand selection: Unwinding the rules. *Wiley Interdiscip Rev RNA* **12**, 1–22 (2021).

52. Frank, F., Sonenberg, N. & Nagar, B. Structural basis for 5′-nucleotide base-specific recognition of guide RNA by human AGO2. *Nature* **465**, 818–822 (2010).

53. Hu, H. Y. *et al.* Sequence features associated with microRNA strand selection in humans and flies. *BMC Genomics* **10**, 413 (2009).

54. Liu, J. *et al.* Argonaute2 is the catalytic engine of mammalian RNAi. *Science* **305**, 1437–1441 (2004).

55. Bartel, D. P. Metazoan MicroRNAs. *Cell* **173**, 20–51 (2018).

56. Kamenska, A. *et al.* The DDX6-4E-T interaction mediates translational repression and P-body assembly. *Nucleic Acids Res* **44**, 6318–6334 (2016).

57. Kaller, M. *et al.* Genome-wide characterization of miR-34a induced changes in protein and mRNA expression by a combined pulsed SILAC and microarray analysis. *Molecular and Cellular Proteomics* **10**, (2011).

58. Chou, C.-H. *et al.* miRTarBase 2016: updates to the experimentally validated miRNA-target interactions database. *Nucleic Acids Res* **44**, D239-47 (2016).

59. Slabáková, E., Culig, Z., Remšík, J. & Souček, K. Alternative mechanisms of MIR-34a regulation in cancer. *Cell Death Dis* **8**, 1–10 (2017).

60. Zhang, H. F., Wang, Y. C. & Han, Y. di. MicroRNA-34a inhibits liver cancer cell growth by reprogramming glucose metabolism. *Mol Med Rep* **17**, 4483–4489 (2018).

61. Llovet, J. M. *et al.* Hepatocellular carcinoma. *Nat Rev Dis Primers* **2**, (2016).

62. Xu, Y. *et al.* Hepatocyte miR-34a is a key regulator in the development and progression of non-alcoholic fatty liver disease. *Mol Metab* **51**, (2021).

63. Kwon, H. *et al.* Epigenetic Silencing of miRNA-34a in Human Cholangiocarcinoma via EZH2 and DNA Methylation: Impact on Regulation of Notch Pathway. *American Journal of Pathology* **187**, 2288–2299 (2017).

64. Parviz, F. *et al.* Hepatocyte nuclear factor 4α controls the development of a hepatic epithelium and liver morphogenesis. *Nat Genet* **34**, 292–296 (2003).

65. Wirsing, A., Senkel, S., Klein-Hitpass, L. & Ryffel, G. U. A systematic analysis of the 3′utr of HNF4A mRNA reveals an interplay of regulatory elements including miRNA target sites. *PLoS One* **6**, (2011).

66. Xu, Y. *et al.* A metabolic stress-inducible miR-34a-HNF4α pathway regulates lipid and lipoprotein metabolism. *Nat Commun* **6**, (2015).

67. Cai, S. H., Lu, S. X., Liu, L. L., Zhang, C. Z. & Yun, J. P. Increased expression of hepatocyte nuclear factor 4 alpha transcribed by promoter 2 indicates a poor prognosis in hepatocellular carcinoma. *Therap Adv Gastroenterol* **10**, 761–771 (2017).

68. Wolff, J. , M. R. , W. P. , C. W. , A. G. , J. A. , & F. P. Direct gene transfer into mouse muscle in vivo. *Science (1979)* **247**, 1465–1468 (1990).

69. Fraley R, S. S. B. P. P. D. Introduction of liposome-encapsulated SV40 DNA into cells. *J Biol Chem* **255**, 10431–5 (1980).

70. Swingle, K. L., Hamilton, A. G. & Mitchell, M. J. Lipid Nanoparticle-Mediated Delivery of mRNA Therapeutics and Vaccines. *Trends Mol Med* **27**, 616–617 (2021).

71. Zatsepin, T. S., Kotelevtsev, Y. v. & Koteliansky, V. Lipid nanoparticles for targeted siRNA delivery - Going from bench to bedside. *Int J Nanomedicine* **11**, 3077–3086 (2016).

72. Kularatne, R. N., Crist, R. M. & Stern, S. T. The Future of Tissue-Targeted Lipid Nanoparticle-Mediated Nucleic Acid Delivery. *Pharmaceuticals* vol. 15 Preprint at https://doi.org/10.3390/ph15070897 (2022).

73. Samaridou, E., Heyes, J. & Lutwyche, P. Lipid nanoparticles for nucleic acid delivery: Current perspectives. *Adv Drug Deliv Rev* **154–155**, 37–63 (2020).

74. Kulkarni, J. A., Witzigmann, D., Leung, J., Tam, Y. Y. C. & Cullis, P. R. On the role of helper lipids in lipid nanoparticle formulations of siRNA. *Nanoscale* **11**, 21733–21739 (2019).

75. Semple, S. C. *et al.* Rational design of cationic lipids for siRNA delivery. *Nat Biotechnol* **28**, 172–176 (2010).

76. Desai, A. S., Hunter, M. R. & Kapustin, A. N. Using macropinocytosis for intracellular delivery of therapeutic nucleic acids to tumour cells. *Philosophical Transactions of the Royal Society B: Biological Sciences* **374**, (2019).

77. Hsu, S. hao *et al.* Cationic lipid nanoparticles for therapeutic delivery of siRNA and miRNA to murine liver tumor. *Nanomedicine* **9**, 1169–1180 (2013).

78. Sasso, J. M. *et al.* The Progress and Promise of RNA Medicine-An Arsenal of Targeted Treatments. *Journal of Medicinal Chemistry* vol. 65 6975–7015 Preprint at https://doi.org/10.1021/acs.jmedchem.2c00024 (2022).

79. Asrani, S. K., Devarbhavi, H., Eaton, J. & Kamath, P. S. Burden of liver diseases in the world. *Journal of Hepatology* vol. 70 151–171 Preprint at https://doi.org/10.1016/j.jhep.2018.09.014 (2019).

80. Ibrahim, S. H., Kamath, B. M., Loomes, K. M. & Karpen, S. J. Cholestatic liver diseases of genetic etiology: Advances and controversies. *Hepatology* vol. 75 1627–1646 Preprint at https://doi.org/10.1002/hep.32437 (2022).

81. Tanimizu, N., Nishikawa, M., Saito, H., Tsujimura, T. & Miyajima, A. Isolation of hepatoblasts based on the expression of Dlk/Pref-1. *J Cell Sci* **116**, 1775–1786 (2003).

82. Zborowski, M. & Chalmers, J. J. Magnetic Cell Separation. in *Methods in molecular biology (Clifton, N.J.)* vol. 32 1–454 (2005).

83. Smirnova, V. V *et al.* Ribosomal leaky scanning through a translated uORF requires eIF4G2. *Nucleic Acids Res* **50**, 1111–1117 (2022).

84. Matlock, B. Assessment of Nucleic Acid Purity. *Technical Bulletin NanoDrop Spectrophotometers* 1–2 (2015).

85. Osborn, J. F. & Daniel, W. W. *Biostatistics: A Foundation of Analysis in the Health Sciences. Journal of the Royal Statistical Society. Series A (General)* vol. 147 (1984).

86. Khan, H. A. ArrayVigil: A Methodology for Statistical Comparison of Gene Signatures Using Segregated-one-tailed (SOT) Wilcoxon's Signed-rank Test. *J Mol Biol* **345**, 645–649 (2005).

87. Piccinin, E. *et al.* Hepatic microRNA expression by PGC-1α and pgc-1β in the mouse. *Int J Mol Sci* **20**, (2019).

88. Joshua M Boucher, A. H. B. R. V. L. L. L. A receptor-specific function for Notch2 in mediating vascular smooth muscle cell growth arrest through cyclin-dependent kinase inhibitor 1B. *Circ Res* **113**, 975–85 (2013).

89. Liang, X., Hart, C. E. & Crooke, S. T. Transfection of siRNAs can alter miRNA levels and trigger non-specific protein degradation in mammalian cells. *Biochimica et Biophysica Acta (BBA) - Gene Regulatory Mechanisms* **1829**, 455–468 (2013).

90. Freier, S. M. & Altmann, K. H. The ups and downs of nucleic acid duplex stability: structure-stability studies on chemically-modified DNA:RNA duplexes. *Nucleic Acids Res* **25**, 4429–4443 (1997).

91. Davis, S., Lollo, B., Freier, S. & Esau, C. Improved targeting of miRNA with antisense oligonucleotides. *Nucleic Acids Res* **34**, 2294–2304 (2006).

92. Hughes, C. S., Postovit, L. M. & Lajoie, G. A. Matrigel: a complex protein mixture required for optimal growth of cell culture. *Proteomics* **10**, 1886–1890 (2010).

93. Belicova, L. *et al.* Anisotropic expansion of hepatocyte lumina enforced by apical bulkheads. *Journal of Cell Biology* **220**, (2021).

94. Shin, D., Pal, S. & Monga, S. Cellular and Molecular Basis of Liver Development Anteroposterior Endoderm Patterning. *Compr Physiol* **3**, 799–815 (2013).

95. Lv, L. *et al.* Self-renewal of hepatoblasts under chemically defined conditions by iterative growth factor and chemical screening. *Hepatology* **61**, 337–347 (2015).

96. Kurien, B. T. & Scofield, R. H. Common artifacts and mistakes made in electrophoresis. *Methods in Molecular Biology* **869**, 633–640 (2012).

97. Xu, Y. *et al.* A metabolic stress-inducible miR-34a-HNF4α pathway regulates lipid and lipoprotein metabolism. *Nat Commun* **6**, (2015).

98. Wang, Y. *et al.* Multiomics Analyses of HNF4α Protein Domain Function during Human Pluripotent Stem Cell Differentiation. *iScience* **16**, 206–217 (2019).

99. Yu, D. *et al.* High fat diet-induced oxidative stress blocks hepatocyte nuclear factor 4α and leads to hepatic steatosis in mice. *J Cell Physiol* **233**, 4770–4782 (2018).

100. Love, K. T. *et al.* Lipid-like materials for low-dose, in vivo gene silencing. *Proc Natl Acad Sci U S A* **107**, 1864–1869 (2010).

101. Sahay, G. *et al.* Efficiency of siRNA delivery by lipid nanoparticles is limited by endocytic recycling. *Nat Biotechnol* **31**, 653–658 (2013).

102. Leboeuf, D. *et al.* Downregulation of the Arg/N-degron Pathway Sensitizes Cancer Cells to Chemotherapy In Vivo. *Molecular Therapy* **28**, 1092–1104 (2020).

103. Feizi, Z. *et al.* Prenatal liver stromal cells: Favorable feeder cells for long-term culture of hepatic progenitor cells. *J Cell Biochem* **120**, 16624–16633 (2019).

104. Salloum-Asfar, S. *et al.* MiRNA-based regulation of hemostatic factors through hepatic nuclear factor-4 alpha. *PLoS One* **11**, (2016).

105. Delaforest, A. *et al.* HNF4A regulates the formation of hepatic progenitor cells from human iPSC-derived endoderm by facilitating efficient recruitment of RNA pol II. *Genes (Basel)* **10**, (2019).

106. Salzman, D. W. *et al.* miR-34 activity is modulated through 5′-end phosphorylation in response to DNA damage. *Nat Commun* **7**, 10954 (2016).

107. Basyuk, E., Suavet, F., Doglio, A., Bordonné, R. & Bertrand, E. Human let-7 stem–loop precursors harbor features of RNase III cleavage products. *Nucleic Acids Res* **31**, 6593–6597 (2003).

108. Marzi, M. J. *et al. Degradation dynamics of microRNAs revealed by a novel pulse-chase approach Running Title: Uncovering miRNA decay in mammalian cells by metabolic labeling*.

109. Haraszti, R. A. *et al.* 5´-Vinylphosphonate improves tissue accumulation and efficacy of conjugated siRNAs in vivo. *Nucleic Acids Res* **45**, 7581–7592 (2017).

110. Elkayam, E. *et al.* siRNA carrying an (E)-vinylphosphonate moiety at the 5´ end of the guide strand augments gene silencing by enhanced binding to human Argonaute-2. *Nucleic Acids Res* **45**, 3528–3536 (2017).

111. Haraszti, R. A. *et al.* 5´-Vinylphosphonate improves tissue accumulation and efficacy of conjugated siRNAs in vivo. *Nucleic Acids Res* **45**, 7581–7592 (2017).

112. Elkayam, E. *et al.* SiRNA carrying an (E)-vinylphosphonate moiety at the 5’ end of the guide strand augments gene silencing by enhanced binding to human Argonaute-2. *Nucleic Acids Res* **45**, 3528–3536 (2017).

113. Prakash, T. P. *et al.* Identification of metabolically stable 5′-phosphate analogs that support single-stranded siRNA activity. *Nucleic Acids Res* **43**, 2993–3011 (2015).

114. Liang, C. A. L. C. Sulfur does not form double bonds in phosphorothioate anions. *J Am Chem Soc* **109**, 6449–6453 (1987).

115. Chen, L., Wang, D., Wu, Z., Ma, L. & Daley, G. Q. Molecular basis of the first cell fate determination in mouse embryogenesis. *Cell Research* vol. 20 982–993 Preprint at https://doi.org/10.1038/cr.2010.106 (2010).

116. Khalil, I. A., Younis, M. A., Kimura, S. & Harashima, H. *Lipid Nanoparticles for Cell-Specific in Vivo Targeted Delivery of Nucleic Acids*. *Biol. Pharm. Bull* vol. 584 (2020).

117. Mangold, K. *Ultrasound-guided in utero lentivirus transduction of the murine nervous system to investigate nervous system disorders*.

118. Hildyard, J. C. W., Wells, D. J. & Piercy, R. J. Identification of qPCR reference genes suitable for normalising gene expression in the developing mouse embryo. *Wellcome Open Res* **6**, 197 (2021).

Annexes

1. Primer design and quality assessment

The efficiency of the used *miR-34a*-LNPs was assessed with RT-qPCR. To proceed with this analysis, primers for the *miR-34a* target genes were designed, and their quality was assessed to ensure reliable results. Primers were designed for the two *miR-34a* target genes, *Hnf4α* and *Notch2*. A primer pair was also constructed to target *Sox9* since it is a cholangiocyte marker. Furthermore, *Gapdh* was the selected housekeeping gene since it is a well-established gene for normalisation in hepatic cells. Moreover, it plays a vital role in the glycolysis pathways, and its expression is stable in E13.5 mice embryos [80].

To assess the specificity and efficiency of the primers, a temperature gradient PCR followed by electrophoresis was performed (Fig. 32). To validate the results, non-template controls (NTC) for each primer were prepared. The NTC is set up precisely as the samples, with master mix and reverse and forward primers, except that no cDNA is added to the solution. However, in the attained NTC *Hnf4α* result, a band appeared on the gel, suggesting a non-specific product (Fig. 32A). The band indicates that the primer pair has dimerised and, thus, is not suitable for RT-qPCR. All the other NTC primer pairs presented no non-specific products. Therefore, they were considered adequate for future analysis. Moreover, the bands in *Hnf4α* 59˚C and *Hnf4α* 61˚C are thicker than usual and have slightly lower molecular weight. This further confirms that the *Hnf4α* primer pair is unsuitable for further analysis. Similarly, the *Gapdh* primer exhibited a lower molecular weight, suggesting that this primer pair amplified a non-specific product. Thus, another housekeeping gene was used for RT-qPCR.

Due to the inadequate result from the previous *Hnf4α* primer pair, four alternative *Hnf4α* primer pairs were assessed via gradient PCR (Fig. 32B). *Hnf4α* 1 had good results with a single band in the wells with cDNA and no bands on the NTC control. However, the attained bands were quite faded. *Hnf4α* 2 gave bands with much lower molecular weight. Therefore, it generated a non-specific product. *Hnf4α* 3 did not show a product on the NTC, and the bands from the wells with cDNA were very bright with the correct molecular weight. Lastly, *Hnf4α* 4 exhibited a thin band at both temperatures, making it unsuitable for further analysis. Overall, *Hnf4α* 3 gave the best results.

The first round of RT-qPCR was performed to assess the quality of the analysed primers. *Hnf4α* 3 and the primer designed for *Notch2* showed non-specific products during the qPCR run. Therefore, they were excluded from future experiments, and other well-established primers available at the lab were used. Furthermore, *B-actin* was elected as an alternative housekeeping gene as *B-actin* is a cytoskeletal component contributing to vital cellular functions [118]. As such, its levels are stable in E13.5 embryonic livers. *B-actin* also demonstrated high efficiency and specificity in the following qPCR round. As such, it was used in the rest of the qPCRs analysis.

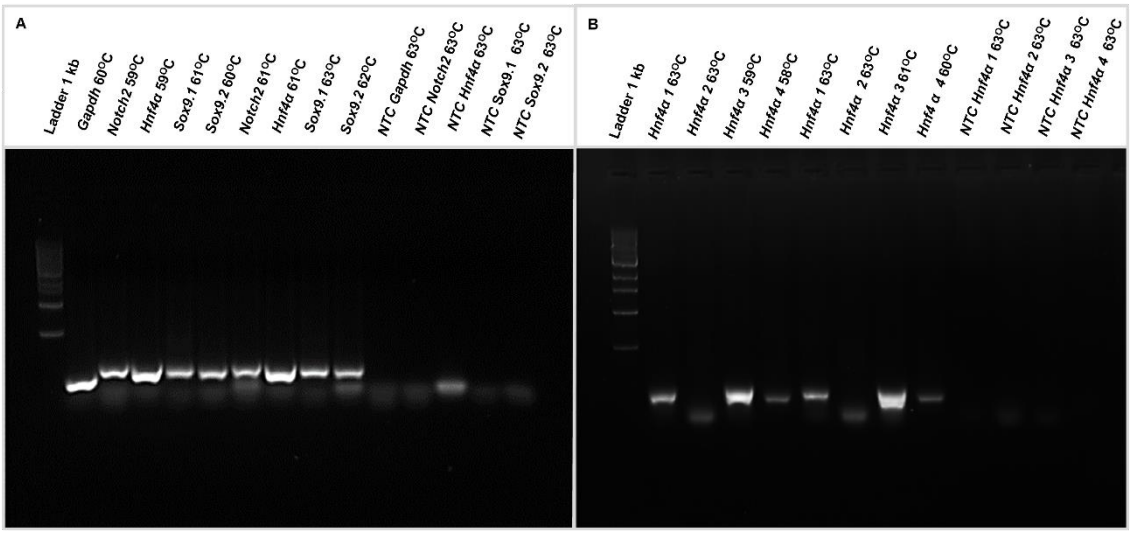

Figure 32 - Primer optimisation results from a temperature gradient PCR followed by electrophoresis. A) Quality assessment for *Gapdh*, *Notch2*, ***Hnf4α*** and *Sox9* (*Sox9*.1 and *Sox9*.2). B) Quality assessment for four ***Hnf4α*** primer pairs ***Hnf4α*** 1, 2, 3 and 4.

Table 2 - Sequences of all the forward and reverse primer pairs (***Hnf4α***, *Notch2*, *Sox9*, *Gapdh* and *B-actin*) that were designed and tested. Marked in bold are the primer pair that were selected for RT-qPCR.

Gene	Forward Primer	Reverse Primer
Hnf4α 1 (*mus musculus*)	TGACCATGGGCAATGACACG	TGTGGTTCTTCCTCACGCTC
Hnf4α 2 (*mus musculus*)	GGAGCCACCAAGAGGTCCAT	ATGATGGCTTTGAGGCAGGC
***Hnf4α* 3 (*mus musculus*)**	**TGCCTGCCTCAAAGCAT**	**CACTCAGCCCCTTGGCAT**
Hnf4α 4 (*mus musculus*)	GAGATGAGCCGTGTGTCCAT	GTACTGCCGGTCGTTGATGTA
Notch2 1 (*mus musculus*)	GGCTACACTTGTCGCTGTTTG	TCTGGGGACACACATCTAGGA
***Notch2* 2 (*mus musculus*)**	**GAACCGTGTGGAGATGAACGAGAC**	**CAGAGGCTGGGAAAGGATGATAGG**
Sox9.1 (*mus musculus*)	CAAAGTTGATCTGAAGCGAGAGG	GTGGTCGTTGGGTGGCAAG
***Sox9*.2 (*mus musculus*)**	**GGCAAAGTTGATCTGAAGCGAG**	**GGTCGTTGGGTGGCAAGTATT**
Gapdh (*mus musculus*)	AGGTCGGTGTGAACGGATTTG	TGTAGACCATGTAGTTGAGGTCA
***B-actin* (*mus musculus*)**	**CCTAGGCACCAGGGTGTGAT**	**CATGTCGTCCCAGTTGGTAA**